



This is a repository copy of *Modelling, simulation and analysis of intensified regenerator for solvent based carbon capture using rotating packed bed technology*.

White Rose Research Online URL for this paper:
<http://eprints.whiterose.ac.uk/118331/>

Version: Accepted Version

Article:

Joel, A.S., Wang, M. orcid.org/0000-0001-9752-270X, Ramshaw, C. et al. (1 more author) (2017) Modelling, simulation and analysis of intensified regenerator for solvent based carbon capture using rotating packed bed technology. *Applied Energy*, 203. pp. 11-25. ISSN 0306-2619

<https://doi.org/10.1016/j.apenergy.2017.05.157>

Article available under the terms of the CC-BY-NC-ND licence (<https://creativecommons.org/licenses/by-nc-nd/4.0/>).

Reuse

This article is distributed under the terms of the Creative Commons Attribution-NonCommercial-NoDerivs (CC BY-NC-ND) licence. This licence only allows you to download this work and share it with others as long as you credit the authors, but you can't change the article in any way or use it commercially. More information and the full terms of the licence here: <https://creativecommons.org/licenses/>

Takedown

If you consider content in White Rose Research Online to be in breach of UK law, please notify us by emailing eprints@whiterose.ac.uk including the URL of the record and the reason for the withdrawal request.



eprints@whiterose.ac.uk
<https://eprints.whiterose.ac.uk/>

1 Modelling, Simulation and Analysis of Intensified 2 Regenerator for Solvent based Carbon Capture using 3 Rotating Packed Bed Technology

4 Atuman S. Joel^a, Meihong Wang^{b*}, Colin Ramshaw^b, Eni Oko^b

5 ^aProcess/Energy Systems Engineering Group, School of Engineering, University of Hull, HU6 7RX, UK

6 ^bDepartment of Chemical and Biological Engineering, University of Sheffield, S1 3JD, UK

7 *Corresponding author. Tel: +44(0) 1142 227160. ; Email address: Meihong.Wang@sheffield.ac.uk

8 9 10 ABSTRACT

11 Intensified regenerator/stripper using rotating packed bed (RPB) for regeneration of
12 rich-MEA solvent in post-combustion CO₂ capture with chemical absorption process
13 was studied through modelling and simulation in this paper. This is the first
14 systematic study of RPB regenerator through modelling as there is no such
15 publication in the open literature. Correlations for liquid and gas mass transfer
16 coefficients, heat transfer coefficient, liquid hold-up, interfacial area and pressure
17 drop which are suitable for RPB regenerator were written in visual FORTRAN as
18 subroutines and then dynamically linked with Aspen Plus[®] rate-based model to
19 replace the default mass and heat transfer correlations in the Aspen Plus[®]. The
20 model now represents intensified regenerator/stripper. Model validation shows good
21 agreement between model predictions and experimental data from literature.
22 Process analyses were performed to investigate the effect of rotor speed on the
23 regeneration efficiency and regeneration energy (including motor power). The rotor
24 speed was varied from 200 to 1200 rpm, which was selected to cover the validation
25 range of rotor speed. Impact of reboiler temperature on the rate of CO₂ stripping was
26 also investigated. Effect of rich-MEA flow rate on regeneration energy and
27 regeneration efficiency was studied. All the process analyses were done for wide
28 range of MEA concentration (32.6 wt%, 50 wt% and 60 wt%). Comparative study
29 between regenerator using packed column and intensified regenerator using RPB
30 was performed and the study shows a size reduction of 9.691 times. This study
31 indicates that RPB process has great potential in thermal regeneration application.

32 **Keywords:** *Post-combustion CO₂ capture, MEA solvent, Process Intensification (PI),*
33 *Rotating Packed Bed (RPB), Process Modelling, Process simulation*

34 1 Introduction

35 1.1 Background

36 Environmental concern has posed many questions as to the impact of greenhouse
37 gas to those changes currently noticed in world climate and the future dangers that

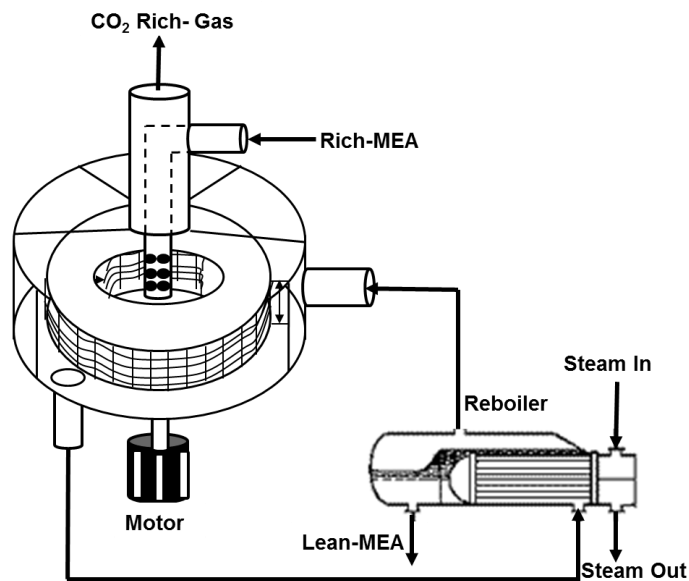
38 will be expected if mitigation measures are not put in place. Combustion of coal and
39 petroleum accounts for the majority of the anthropogenic CO₂ emissions. Petroleum
40 is mostly used as a transportation fuel for vehicles while coal is used mostly for
41 electricity generation, for instance about 85.5% of coal is used for electricity
42 generation in 2011 in the UK [1]. Albo *et al.* [2] stated that among the greenhouse
43 gases, CO₂ contributes to more than 60% of global warming. Statistics from World
44 Metrological Organisation (WMO) showed the amount of CO₂ in the atmosphere
45 reached 393.1 ppm in 2012. The WMO report also showed that the amount of CO₂ in
46 the atmosphere has increased on average by 2 ppm per year for the past 10 years.
47 Recent report by CO₂-Earth [3] shows that as at 8 April 2017 CO₂ atmospheric
48 concentration stood at 407.78 ppm, this increased atmospheric concentration of CO₂
49 affects the radiative balance of the earth surface [4].

50 In order to meet the set target of 50% emission reduction by 2050 as compared to
51 the level of 1990 as proposed by Intergovernmental panel on climate change (IPCC)
52 [5], carbon capture and storage (CCS) is an important option for that target to be
53 achieved. The International Energy Agency (IEA) [6] identifies CCS as a significant
54 and low-cost option in fighting climate change. The most matured CO₂ capture
55 technology is post-combustion CO₂ capture (PCC) based on chemical absorption as
56 reported in Mac Dowell *et al.* [7] which is also believed to be a low-risk technology
57 and promising near-term option for large-scale CO₂ capture.

58 PCC for coal-fired power plants using conventional packed columns has been
59 reported by many authors. Dugas [8] carried out pilot plant study of PCC in the
60 context of fossil fuel-fired power plants. Lawal *et al.* [9-11] carried out dynamic
61 modelling and process analysis of CO₂ absorption for PCC in coal-fired power
62 plants. In all these studies, one of the identified challenges to the commercial roll-out
63 of the technology has been the high capital and operating costs which has an
64 unavoidable impact on electricity cost. Systematic study of aqueous
65 monoethanolamine (MEA)-based CO₂ capture process looking at the techno-
66 economic assessment of the MEA process and its improvements was reported by Li
67 *et al.* [12]. Oh *et al.* [13] study energy minimization of MEA-based CO₂ capture
68 process it was found that Flue gas splitting gives a significant reduction of energy
69 consumption. Solvent performance comparison for a large scale pulverized coal
70 power plant was reported by Sharifzadeh *et al.* [14]. Hanak *et al.* [15] reported
71 efficiency improvements for the coal-fired power plant retrofit with CO₂ capture plant
72 using chilled ammonia process showing efficiency penalty reduced to 8.7%. Also
73 Zhao *et al.* [16] using mixed solvent for 650 MW power plant reported that the net
74 power efficiency penalty was reduced from 9.13% to 7.66%. Approaches such as
75 heat integration, inter-cooling among others could reduce the operating cost slightly.
76 However, they limit the plant flexibility and will make operation and control more
77 difficult [17]. Process intensification (PI) has the potential to meet this challenge [18-
78 20].

79 Study of intensified absorber was reported in Joel *et al* [21,22] and Agarwal *et al.*
 80 [23]. Joel *et al* [21] reported 12 times volume reduction for absorber if using RPB
 81 technology as compared to packed column. Results from Agarwal *et al.* [23]
 82 indicated 7 times volume reduction when using RPB as compared to conventional
 83 packed column. The study by Joel *et al.* [21] uses aqueous MEA solvent while
 84 Agarwal *et al.* [23] uses diethanolamine (DEA) as solvent. This is the main reason for
 85 the differences in size reduction since faster reaction rate means shorter residence
 86 time and slower reaction rate means longer residence time required for the same
 87 capture rate. Jassim *et al.* [24] and Cheng *et al.* [25] reported experimental studies
 88 on intensified regenerator using RPB. Zhao *et al.* [26] study the mass transfer
 89 performance of CO₂ capture in rotating packed bed and Chamchan *et al.* [27]
 90 compared RPB and PB absorber in pilot plant.

91 Figure 1 is a typical process flow diagram of an intensified regenerator using RPB for
 92 solvent regeneration. The flowsheet was used by Jassim *et al.* [24] and Cheng *et al.*
 93 [25] for experimental study. One of the operational benefits of using RPB is its ability
 94 to be operated at higher gas and/or liquid flow rates owing to the low tendency of
 95 flooding compared to that in the conventional packed bed [28]. Another benefit of
 96 using RPB is its better self-cleaning, avoidance of blocking in the system, and being
 97 unaffected by a moderate disturbance in its orientation [29].



98
 99 Figure 1 Schematic diagram of an RPB regenerator

100

101 **Nomenclature**

- a effective interfacial area (m²/m³)
- a_i activity of species *i* in a solution
- a_t total specific surface area of packing (m²/m³)
- a_w wetted area per unit volume (m²/m³)

a'_p	parameter for Chen et al. [24] and Chen [25] correlations for liquid and gas film mass transfer coefficients (= 3000 m ² /m ³)
c	width of wire mesh packing opening (mm)
C_i^l	concentration of component i
Cp_i	heat capacity for component i
d	wire diameter of wire mesh packing (mm)
D	column diameter (m)
D_G	diffusivity of gas (m ² /s)
D_L	diffusivity of liquid (m ² /s)
E_j	activation energy (kJ/mol)
d_p	packing size (m)
G	volumetric gas flow rate (m ³ /s)
G^m	Gas molar flowrate (kmol/s)
g_c	gravitational acceleration or acceleration due to centrifugal field (m ² /s)
g_o	characteristic acceleration value (100 m ² /s)
H	height of packing (m)
h_G	gas phase specific molar enthalpy (J/kmol)
h_L	liquid phase specific molar enthalpy (J/kmol)
$h_{g/l}$	interfacial heat transfer coefficient (W/m ² K)
ΔH_r	heat of desorption of CO ₂ (J/kmol)
ΔH_{vap}	heat of vaporisation of H ₂ O (J/kmol)
k_G	gas film mass transfer coefficient (m/s)
K_G^a	overall mass transfer coefficient (1/s)
k_j^o	pre-exponential factor (kmol/m ³ .s)
k_L	liquid film mass transfer coefficient (m/s)
L	Liquid mass flowrate per tangential area (kg/m ² /s)
L^m	Liquid molar flowrate (kmol/s)
MEA	Monoethanolamine
N_i	molar fluxes for component i (kmol/m ² s)
P_{motor}	motor power (kilowatts)
Q_L	volumetric flow rate of liquid (m ³ /s)
r	radial position (m)
R_c	ideal gas constant (J kmol ⁻¹ K ⁻¹)
r_j	reaction rate for reaction j
rxn_i	reaction rate of component i , (kmol/m ³ /s)

r_i	inner radius of the RPB (m)
r_o	outer radius of the RPB (m)
r_s	radius of the stationary housing of the RPB (m)
T	temperature (K)
t_{res}	residence time (s)
u_l	superficial liquid velocity (m/s)
u_g	superficial gas velocity (m/s)
U_o	characteristic superficial liquid velocity (1cm/s)
V	volume of the liquid films in the RPB (m ³)
V_i	volume inside the inner radius of the RPB = $\pi r_i^2 Z$ (m ³)
V_o	volume between the outer radius of the bed and the stationary housing = $\pi(r_s^2 - r_o^2)Z$ (m ³)
V_t	total volume of the RPB = $\pi r_s^2 Z$ (m ³)
x_i	Component molar fraction in liquid phase
y_i	Component molar fraction in gas phase
$y_{CO_2,in}$	mole fraction of CO ₂ in inlet gas stream
$y_{CO_2,out}$	mole fraction of CO ₂ in outlet gas stream
Z	axial height of the RPB (m)

102

Greek letters

α_{ij}	reaction order of species i in reaction j
ε	porosity of packing, m ³ /m ³
ε_L	liquid holdup (m ³ /m ³)
μ	viscosity (Pa.s)
ρ_L	liquid density (kg/m ³)
ρ_G	gas density (kg/m ³)
σ	liquid surface tension (N/m)
σ_c	critical surface tension (N/m)
σ_w	surface tension of water (N/m)
ν_L	kinematic liquid viscosity (m ² /s)
ν_G	kinematic gas viscosity (m ² /s)
ω	angular velocity (rad/s)

103

Dimensionless groups

Fr_L	liquid Froude number ($u_l^2 a_t / g_c$)
Gr_G	gas Grashof number ($d_p^3 g_c / \nu_G^2$)

Gr_L	liquid Grashof number ($d_p^3 g_c / \nu_L^2$)
Re_G	gas Reynolds number ($u_g / a_t \nu_G$)
Re_L	liquid Reynolds number ($u_l / a_t \nu_L$)
Sc_L	liquid Schmidt number (ν_L / D_L)
We_L	liquid Webber number ($u_l^2 \rho_L / a_t \sigma$)
ϕ	theoretical probability of liquid uncaptured by fibers ($c^2 / (d + c)^2$)

104 1.2 Motivation

105 Over 8,000 tonnes of CO₂ per day will be released from a typical 500 MWe
 106 advanced supercritical coal fired power plant operating at 46% overall net power
 107 plant efficiency (LHV basis) [30]. This huge volume of flue gas will require big column
 108 size. Lawal *et al.* [9] reported dynamic modelling study of a 500 MWe sub-critical
 109 coal-fired power plant using the packed column (i.e. conventional technology). From
 110 the study, one regenerator of 17m in packing height and 9 m in diameter will be
 111 needed for regeneration of rich-MEA solvent. This huge packed column will mean
 112 higher capital and operating costs, therefore a technological option leading to smaller
 113 equipment size is very important. Kothandaraman *et al.* [31] reported that in
 114 conventional packed tower majority (approximately 62%) of the energy consumed
 115 during the CO₂ capture process was used for the solvent regeneration, therefore it is
 116 necessary to look for technological options that will reduce this energy requirement.

117 1.3 Novel contributions of the paper

118 This is the first systematic study on RPB regenerator through modelling as there is
 119 no such publication in the open literature. There are four novel aspects in this paper:
 120 (a) A new first principle model for intensified regenerator using RPB was developed
 121 which was implemented in Aspen Plus® rate-based model by replacing different
 122 correlations for mass transfer, interfacial area and liquid hold-up. Steady state
 123 validation of the intensified regenerator is performed using experimental data from
 124 Jassim *et al.* [24] and Cheng *et al.* [25]. (b) Process analysis of the intensified
 125 regenerator involving different process scenarios were carried out to gain insights for
 126 process design and operation. These process scenarios are: (i) the impact of
 127 rotational speed on the regeneration efficiency and regeneration energy at fixed
 128 intensified regenerator size and rich-MEA flow rate was studied; (ii) the effect of rich-
 129 MEA solvent flow rate on the regeneration efficiency and regeneration energy was
 130 explored; (iii) the effect of reboiler temperature on regeneration efficiency and
 131 regeneration energy was explored. (c) Comparative study was performed between
 132 intensified regenerator using RPB and conventional regenerator using packed bed. It
 133 was found that there is 9.69 times reduction in size under the same conditions which
 134 means decrease in equipment capital cost. (d) The study were done over wide range

135 of MEA concentrations (32.6 wt%, 50 wt% and 60 wt%) and the energy consumption
136 per ton of CO₂ is within the range of conventional packed column.

137 **2 Model Development**

138 Model for intensified regenerator using RPB does not exist in any commercially
139 available model library (including Aspen Plus®). To model intensified regenerator
140 using RPB, the default mass/heat transfer correlations in the Aspen Plus® rate-based
141 model have to be replaced with subroutines written in Intel® visual FORTRAN. The
142 new model now represents an intensified regenerator using RPB. The new steady
143 state model is still developed based on two-film theory Joel *et al.* [21]. The
144 correlations include: liquid phase mass transfer coefficient given by Chen *et al.* [32],
145 gas-phase mass transfer coefficient given by Chen [33], interfacial area correlation
146 estimated by Luo *et al.* [34] and liquid hold-up correlation given by Burns *et al.* [35].
147 Dry pressure drop expression was used since it accounts in an additive manner of
148 the drag and centrifugal forces, the gas-solid slip and radial acceleration effect [36].

149 2.1 *Main governing equations*

150 The main governing equations include material and energy balance equations.
151 Momentum balance is reflected in the pressure drop relation presented in Section
152 2.7.

153 2.1.1 *Gas and liquid phase material balances*

154 Assuming steady state conditions, material balances for gas and liquid phase in the
155 RPB is described by Equations 1 and 2. Due to flow directions in RPB, the equations
156 are based on numerical discretisation in the radial direction. Also, the term $2\pi rZ$ is
157 described preferably as tangential area to differentiate it from cross sectional area as
158 it varies from section to section along the radial direction.

159 Material balances for gas phase:

$$160 \quad 0 = \frac{1}{2\pi rZ} \frac{\partial(G^m y_i)}{\partial r} - aN_i \quad (1)$$

161 Material balances for liquid phase:

$$162 \quad 0 = -\frac{1}{2\pi rZ} \frac{\partial(L^m x_i)}{\partial r} + aN_i + \epsilon_L rxn_i \quad (2)$$

163 The equation includes component molar flow balances (represented by the
164 derivative terms) across each radial segment per tangential area, interfacial molar
165 fluxes (aN_i) and liquid phase reaction rate ($\epsilon_L rxn_i$). By this, reactions are deemed to
166 occur only in the liquid phase and ionic components therefore only exist in the liquid
167 phase.

168 *2.1.2 Gas and liquid phase energy balances*

169 Energy balances for gas and liquid phase is given by Equations 3 and 4 respectively
170 [37]

171 Energy balances for gas phase:

$$172 \quad 0 = \frac{1}{2\pi r Z} \frac{\partial(G^m h_G)}{\partial r} - a h_{g/l} (T_l - T_g) - Q_G^{Loss} \quad (3)$$

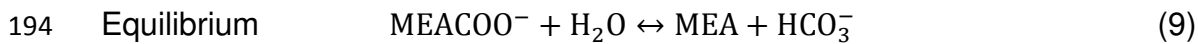
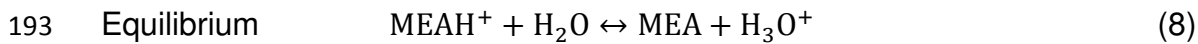
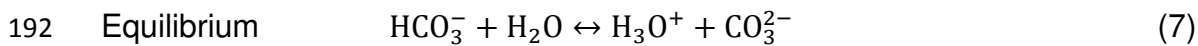
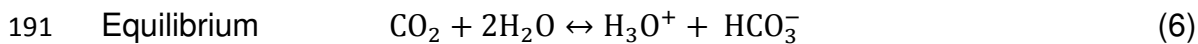
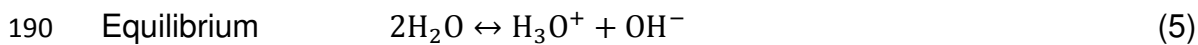
173 Energy balances for liquid phase:

$$174 \quad 0 = -\frac{1}{2\pi r Z} \frac{\partial(L^m h_L)}{\partial r} - a (h_{g/l} (T_l - T_g) - \Delta H_r N_{CO_2} - \Delta H_{vap} N_{H_2O}) - Q_L^{Loss} \quad (4)$$

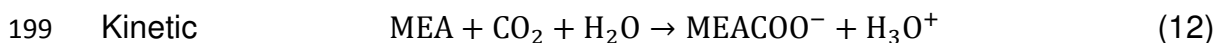
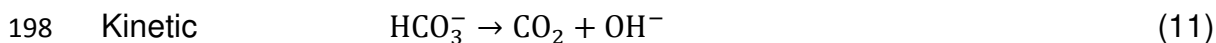
175 The equations include interfacial heat transfer, $h_{g/l}(T_l - T_g)$, heat released due to
176 CO₂ desorption from the loaded MEA solvent, $\Delta H_r N_{CO_2}$ and heat released or
177 absorbed due to H₂O condensation or vaporization, $\Delta H_{vap} N_{H_2O}$, [17]. Due to the
178 relatively higher temperature of the stripper compared to ambient condition, heat
179 losses (Q_G^{Loss} and Q_L^{Loss}) are also taken into account.

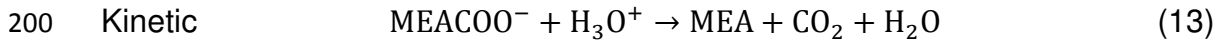
180 *2.2 Physical property*

181 Electrolyte Non-Random-Two-Liquid (ElecNRTL) activity coefficient model in Aspen
182 Plus® was used to describe the vapour–liquid equilibrium, the chemical equilibrium
183 and the physical properties of the system. The equilibrium constants for reactions 5-
184 9 are calculated from the standard Gibbs free energy change, the equilibrium
185 reactions are assumed to occur in the liquid film and kinetic reactions equations and
186 parameters are obtained from AspenTech [38]. The electrolyte solution chemistry
187 which is used in property calculation is modelled with chemistry model and all the
188 ionic reactions are assumed to be in chemical equilibrium as shown in Equations 5-9
189 [38].



195 Kinetic reactions used for the intensified stripping calculation is specified by
196 Equations 10-13 in the reaction part of the regenerator model in the Aspen Plus.





201 Power law expression Equation 14 is used for the rate-controlled reactions. The
 202 kinetic parameters for reactions in Equations 10-13 were listed in Table 1

203
$$r_j = k_j^o \exp\left(-\frac{E_j}{R_c} \left[\frac{1}{T} - \frac{1}{298.15}\right]\right) \prod_{i=1}^N a_i^{\alpha_{ij}}$$
 (14)

204 Table 1 Constants for power law expressions for the absorption of CO₂ by MEA [39]

Reaction No.	k_j^o (kmol/m ³ .s)	E_j , kJ/mol
10	1.33e+17	55.38
11	6.63e+16	107.24
12	3.02e+14	41.2
13	6.56e+27	95.24

205

206 **2.3 Liquid phase mass transfer coefficient**

207 An expression was introduced by Tung and Mah [40] based on penetration theory to
 208 describe the liquid mass transfer behaviour in the RPB.

209
$$\frac{k_L d_p}{D_L} = 0.919 \left(\frac{a_t}{a}\right)^{1/3} Sc_L^{1/2} Re_L^{2/3} Gr_L^{1/6}$$
 (15)

210 This correlation was developed without considering the Coriolis force or the effect of
 211 the packing geometry. This is why there is a need for an alternative correlation for
 212 liquid phase mass transfer coefficient.

213 Chen *et al.* [32] developed liquid phase mass transfer correlation considering the end
 214 effect and packing geometry. The correlation was found to be valid for different sizes
 215 of the RPBs and for viscous Newtonian and non-Newtonian fluids. Because of these
 216 advantages, Equation 16 is selected for calculating the liquid phase mass transfer
 217 coefficient, and also findings from Joel *et al.* [22] suggested the use of Equation 16
 218 because of its smaller error prediction.

219

220
$$\frac{k_L a d_p}{D_L a_t} \left(1 - 0.93 \frac{V_o}{V_t} - 1.13 \frac{V_i}{V_t}\right) = 0.35 Sc_L^{0.5} Re_L^{0.17} Gr_L^{0.3} We_L^{0.3}$$

 221
$$\left(\frac{a_t}{a_p}\right)^{-0.5} \left(\frac{\sigma_c}{\sigma_w}\right)^{0.14}$$
 (16)

222

223 **2.4 Gas phase mass transfer coefficient**

224 Onda *et al.* [41] correlation for calculating gas-side mass transfer coefficient
 225 (Equation 17) was developed for conventional packed column. Sandilya *et al.* [42]
 226 suggested that the gas rotates like a solid body in the rotor because of the drag force

227 caused by the packing, which means that gas-side mass transfer coefficient should
 228 be similar to that in a conventional packed column, but the end effect and packing
 229 effect were not considered, this makes the authors to select Equation 18 proposed
 230 by Chen [33] instead of Equation 17.

$$231 \quad k_G = 2.0(a_t D_G) Re_G^{0.7} Sc_G^{1/3} (a_t d_p)^{-2} \quad (17)$$

232 Chen [33] presented local gas-side mass transfer coefficient correlation using two-
 233 film theory for RPB. Equation 18 for calculating the gas phase mass transfer
 234 coefficient was used in the model because it accounts for the effect of rotation of the
 235 RPB.

$$236 \quad \frac{k_G a}{D_G a_t^2} \left(1 - 0.9 \frac{V_o}{V_t}\right) = 0.023 Re_G^{1.13} Re_L^{0.14} Gr_G^{0.31} We_L^{0.07} \left(\frac{a_t}{a'_p}\right)^{1.4} \quad (18)$$

237 238 2.5 Total gas-liquid interfacial area

239 Total gas-liquid interfacial area correlation for conventional packed column was
 240 developed by Onda *et al.* [41] as shown in Equation 19. It can be modified to account
 241 for the effect of rotation of the bed but because it is not originally designed for RPB
 242 and also it was not designed for different types of packing, Equation 20 developed by
 243 Luo *et al.* [34] was selected.

$$244 \quad \frac{a}{a_t} = 1 - \exp \left[-1.45 \left(\frac{\sigma_c}{\sigma}\right)^{0.75} Re_L^{0.1} We_L^{0.2} Fr_L^{-0.05} \right] \quad (19)$$

245 Luo *et al.* [34] studied gas-liquid effective interfacial area in an RPB considering
 246 different types of packing, also taking into account the effect of fibre diameter and
 247 opening of the wire mesh.

$$248 \quad \frac{a}{a_t} = 66510 Re_L^{-1.41} Fr_L^{-0.12} We_L^{1.21} \varphi^{-0.74} \quad (20)$$

249 2.6 Liquid hold-up

250 Liquid holdup correlation given by Burns *et al.* [35] was used. The correlation is
 251 based on data obtained through measurement of electrical resistance across
 252 sections of an RPB. The study showed that the liquid hold-up is approximately
 253 inversely proportional to the local packing radius and is largely independent of gas
 254 flow up to the flooding point and also liquid viscosity has only a weak influence on
 255 hold-up [35].

$$256 \quad \epsilon_L = 0.039 \left(\frac{g_c}{g_o}\right)^{-0.5} \left(\frac{u_t}{U_o}\right)^{0.6} \left(\frac{v_L}{v_o}\right)^{0.22} \quad (21)$$

257 $g_o = 100 \text{ m s}^{-2}, \quad U_o = 1 \text{ cm s}^{-1}, \quad v_o = 1 \text{ cS} = 10^{-6} \text{ m}^2 \text{ s}^{-1}$

258 $u_l = \frac{Q_L}{2\pi r Z}$ (22)

259 **2.7 Dry pressure drop expression**

260 Semi-empirical dry pressure drop expression was given by Llerena-Chavez and
 261 Larachi [36]. The correlation was developed based on Ergun-type semi-empirical
 262 relationships in which the gas-slip and radial acceleration effects, the laminar and
 263 inertial drag effects and the centrifugal effect were aggregated additively to form the
 264 pressure drops correlation in the RPB [36].

265
$$\Delta P_{Packed\ bed} = \frac{150(1-\varepsilon)^2\mu}{d^2\varepsilon^3} \left(\frac{G}{2\pi Z}\right) \ln \frac{r_o}{r_i} + \frac{1.75(1-\varepsilon)\rho}{d\varepsilon^3} \left(\frac{G}{2\pi Z}\right)^2 \left(\frac{1}{r_i} - \frac{1}{r_o}\right)$$

266
$$+ \frac{1}{2}\rho\omega^2(r_o^2 - r_i^2) + F_c$$
 (23)

267 where F_c is a corrective function given as:

268 $F_c = \varepsilon(a - G + (b + \omega^c)G^2)$ (24)

269 a, b, and c are fitting parameters given as:

270 $a = -0.08 \text{ m}^3/\text{s} \quad b = 2000(\text{rpm})^c \quad c = 1.22$

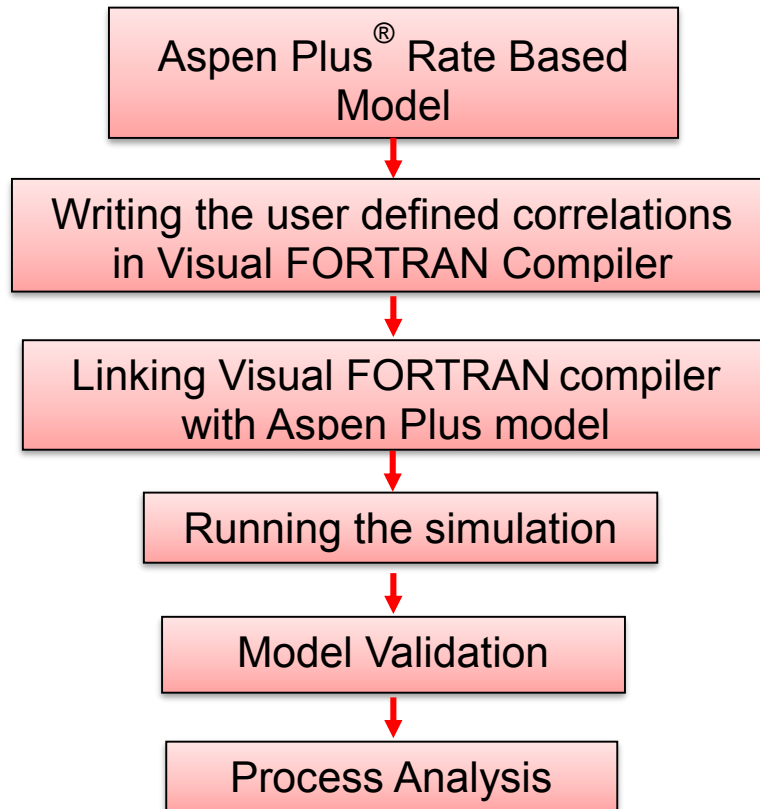
271 **2.8 Power consumption by RPB stripper motor**

272 The amount of power consumed by motor for rotating RPB absorber and stripper is
 273 calculated using the correlation proposed by Singh *et al.* [43]. The correlation was
 274 used to account for all the frictional losses and also the power required for
 275 accelerating the liquid entering the packing bed to the rotational speed at the outer
 276 radius. It is important to note that frictional losses are highly dependent upon the
 277 design of the machine and cannot be predicted without advance knowledge of the
 278 design (i.e., type of bearings, direct or pulley drive, etc.) [43].

279 $P_{motor} = 1.2 + 1.1 \times 10^{-3} \rho_L r_o^2 \omega^2 Q_L$ (25)

280 2.9 Modelling and simulation methodology

281 The procedure used in this paper for modelling and simulation of the RPB is shown
 282 in **Figure 2** and summary of the model parameters and correlations were presented
 283 in **Table 2**



284

Figure 2 Methodology used in this paper [21,22]

285

286 Table 2 Summary of model parameters

Parameters	Correlations or values	
	Jassim <i>et al</i>	Cheng <i>et al</i>
Model geometry		
r_i (m)	0.156	0.076
r_o (m)	0.398	0.160
h (m)	0.025	0.020
surface area of the packing per unit volume of the bed (m^2/m^3)	2132	803
Liquid phase mass transfer coefficient	See Equation 16	
Gas phase mass transfer coefficient	See Equation 18	
Total gas-liquid interfacial area	See Equation 20	
Liquid holdup	See Equation 21	
Dry pressure drop expression	See Equation 23	
Motor power	See Equation 25	

287 **3 Model Validation**

288 3.1 *Model validation using experimental data from Jassim et al. [24]*

289 The experimental data used for the model validation was obtained from Jassim *et al.*
 290 [24]. From their experiments, rich-MEA concentration of 32.9 wt%, 35.7 wt%, 30.8
 291 wt%, 57.4 wt% and 52 wt% were selected for the validation study. The equipment
 292 specifications and process input conditions for the validation study are shown in
 293 **Tables 3 and 4**. The study was done under two different rotor speeds 800 rpm and
 294 1000 rpm.

295 Table 3 RPB stripper packing specifications used by Jassim et al. [24]

Description	Value
RPB outer diameter	0.398 m
RPB inner diameter	0.156 m
RPB axial depth	0.025 m
Packing specific surface area	2132 m ² /m ³
Packing porosity	0.76

296 Table 4 Input process conditions for Run 1 to Run 5 [24]

	Runs				
	Run 1	Run 2	Run 3	Run 4	Run 5
Rotor speed (RPM)	800	800	800	1000	1000
Rich-MEA temperature (°C)	67.100	69.000	70.000	57.200	58.400
Rich-MEA pressure (kPa)	101.325	101.325	101.325	101.325	101.325
Rich-MEA flow rate (kg/s)	0.200	0.200	0.400	0.400	0.200
Rich-MEA composition (wt. %)					
H ₂ O	58.116	54.013	61.536	25.142	32.895
CO ₂	8.984	10.287	7.664	17.458	15.105
MEA	32.900	35.700	30.800	57.400	52.000
Rich-MEA CO ₂ loading (mol CO ₂ /mol MEA)	0.3790	0.3999	0.3454	0.4221	0.4030

297

298 Table 5 Simulation results compared to experimental data [24] for Run 1 to Run 5

	Runs				
	Run 1	Run 2	Run 3	Run 4	Run 5
Rotor speed (RPM)	800	800	800	1000	1000
Experimental measurement					
Lean-MEA CO ₂ loading (mol/mol)	0.321	0.329	0.329	0.403	0.334
Model prediction					
Lean-MEA CO ₂ loading (mol/mol)	0.316	0.295	0.298	0.355	0.320
Relative error (%)	1.558	10.334	9.422	11.911	4.192

299
 300 Model validation is shown in **Table 5** which gives percentage error prediction of not
 301 more than 12 % on the lean-MEA CO₂ loading. The lean-MEA CO₂ loading was
 302 evaluated on mole basis as shown in Equation 26.

303
$$\text{Loading} = \frac{\text{Moles of all CO}_2 \text{ carrying species}}{\text{Moles of all MEA carrying species}} = \frac{[CO_2] + [HCO_3^-] + [CO_3^{2-}] + [MEACOO^-]}{[MEA] + [MEA^+] + [MEACOO^-]} \quad (26)$$

304 Jassim *et al.* [24] didn't include experimental results on reboiler duty, therefore the
 305 authors cannot compare model predictions with experimental tests.

306 **3.2 Model validation based on experimental data from Cheng et al. [25]**

307 Cheng et al [25] carried out experimental study on the thermal regeneration of
 308 alkanolamines solutions in a RPB using 30 wt% MEA aqueous solution loaded with
 309 CO₂ and a CO₂ - loaded aqueous solution consisting of 20 wt% diethylenetriamine
 310 and 10 wt% piperazine. For the purpose of this study, experimental data with 30 wt%
 311 MEA aqueous solution was used for model validation. RPB stripper specifications
 312 and process input conditions for the model are shown in **Tables 6 and 7**.

313 Table 6 RPB stripper packing specifications used by Cheng et al [25]

Description	Value
RPB outer diameter	0.160 m
RPB inner diameter	0.076 m
RPB axial depth	0.020 m
Packing specific surface area	803 m ² /m ³
Packing porosity	0.960

314 Table 7 Input process conditions for different reboiler temperature [25]

Variable	Reboiler Temperature		
	105 °C	115 °C	120 °C
Rotor speed (RPM)	900	900	900
Rich-MEA temperature (°C)	96.6	97	97
Rich-MEA pressure (kPa)	202.65	202.65	202.65
Rich-MEA flow rate (mL/min)	400	400	400
Rich-MEA CO ₂ loading (mol CO ₂ /mol MEA)	0.484	0.484	0.484

315 Table 8 Simulation results compared to experimental data [25]

Variable		Reboiler Temperature (°C)		
		105	115	120
Lean Loading (mol CO ₂ /mol MEA)	Experimental measurement	0.418	0.340	0.271
	Model prediction	0.423	0.367	0.289
	Relative error (%)	1.132	8.054	6.848
Reboiler duty (kW)	Experimental measurement	0.620	0.900	1.240
	Model prediction	0.629	0.989	1.383
	Relative error (%)	1.487	9.951	11.498

316 Model results compared with the experimental data from Cheng *et al.* [25] shown in
 317 **Table 8** indicates a good agreement with relative error on lean loading of less than
 318 9% and reboiler duty percentage error of less than 12% for different reboiler
 319 temperatures.

320 In summary, the model has predicted all experimental data reasonably well with not
 321 more than 12% error prediction, the model developed can then be used to carry out
 322 process analysis in order to study the system behaviour when there is a change in
 323 some variables.

324 4 Process Analysis

325 With the validated models, we carried out process analysis to explore the effect of
 326 rich-MEA flow rate, rotor speed and reboiler temperature on (a) the regeneration
 327 efficiency calculated based on loading (Equation 27) and calculated based on
 328 amount of CO₂ in rich-MEA and lean-MEA solvent (Equation 28), (b) the
 329 regeneration energy (with and without motor power) expressed in Equations 29 and
 330 30 respectively. But the electricity power consumed by motor is high grade while the
 331 steam power in the reboiler is a low grade, therefore for the two powers to be
 332 comparable, efficiency loss needs to be accounted for by multiplying the motor

333 power with 2.5 (i.e. assuming 40% thermal efficiency in converting thermal heat into
 334 electricity. The reason is that solvent-based carbon capture can be used in different
 335 scenarios such as coal-fired subcritical power plants, coal-fired supercritical power
 336 plants, gas-fired power plants and other industrial manufacturing plants. 40% is a
 337 good assumption for these different scenarios). Equations 31 and 32 were used to
 338 estimate the solvent residence time in the RPB with the assumption that wetted area
 339 per unit volume is equal to specific surface area of the packing [44]. The RPB
 340 stripper used for the process analysis has the following packing geometry: outer
 341 radius = 0.371 m; inner radius = 0.152 m; axial depth of packing = 0.167 m; packing
 342 void fraction = 0.76; packing specific surface area = 2,132 m²/m³.

$$343 \text{ Regeneration eff. 1} = \left(\frac{\text{Rich CO}_2 \text{ loading} - \text{Lean CO}_2 \text{ loading}}{\text{Rich CO}_2 \text{ loading}} \right) \times 100 \quad (27)$$

$$344 \text{ Regeneration eff. 2} = \left(\frac{\text{Amount of CO}_2 \text{ in Rich} - \text{Amount of CO}_2 \text{ in Lean}}{\text{Amount of CO}_2 \text{ in Rich}} \right) \times 100 \quad (28)$$

$$345 \text{ Regeneration energy (without motor power)} = \frac{\text{Reboiler duty}}{\text{Mass of CO}_2 \text{ desorbed}} \quad (29)$$

$$346 \text{ Regeneration energy (with motor power)} = \frac{(\text{Reboiler duty} + P_{\text{motor}} \times 2.5)}{\text{Mass of CO}_2 \text{ desorbed}} \quad (30)$$

$$347 \text{ Residence time (t}_{\text{res}}) = \frac{V}{Q_L} \quad (31)$$

348 Where

$$349 V = \left(\frac{3v_L Q_L}{2\pi Z a_w \omega^2} \right)^{1/3} (a_w 2\pi Z) \left[r_o^{4/3} - r_i^{4/3} \right] \quad (32)$$

350 Q_L = liquid volumetric flowrate (m³/s)

351

352 4.1 *Effect of rich solvent flow rate on regeneration efficiency and energy*

353 4.1.1 *Justification for case study*

354 Rich-MEA solvent flow rate not only has influence on the amount of CO₂ that will be
 355 stripped off from the regenerator, but also has relationship with the reboiler duty.
 356 Therefore study on the right quantity of rich-MEA solvent coming into the regenerator
 357 of fixed or given size is necessary.

358 *4.1.2 Setup of the case study*

359 For this study, the process input conditions are shown in Table 9 with the rich-MEA
 360 flow rate varying from 0.2 kg/s to 0.8 kg/s. Here the rich-MEA loading is kept
 361 constant (i.e. 0.482 mol CO₂/mol MEA). Also in this study lean-MEA loading and
 362 reboiler temperature are the two outputs parameters that were maintained at 0.3178
 363 mol CO₂/mol MEA and 120 °C respectively. Reboiler temperature is maintained at
 364 120 °C by controlling the back pressure regulator to the stripper.

365 Table 9 Process inputs

Variable	Case 1	Case 2	Case 3
Rich-MEA temperature (°C)	104	104	104
Rich-MEA pressure (kPa)	202.650	202.650	202.650
Rich-MEA flow rate (kg/s)	0.2 – 0.8	0.2 – 0.8	0.2 – 0.8
Rich-MEA composition (wt. %)			
H ₂ O	56.072	32.027	18.559
CO ₂	11.328	17.530	21.010
MEA	32.600	50.443	60.431
Rich loading (mol CO ₂ /mol MEA)	0.482	0.482	0.482
Reboiler temperature (°C)	120	120	120
Rotor speed (RPM)	1000	1000	1000

366

367 *4.1.3 Results and discussion*

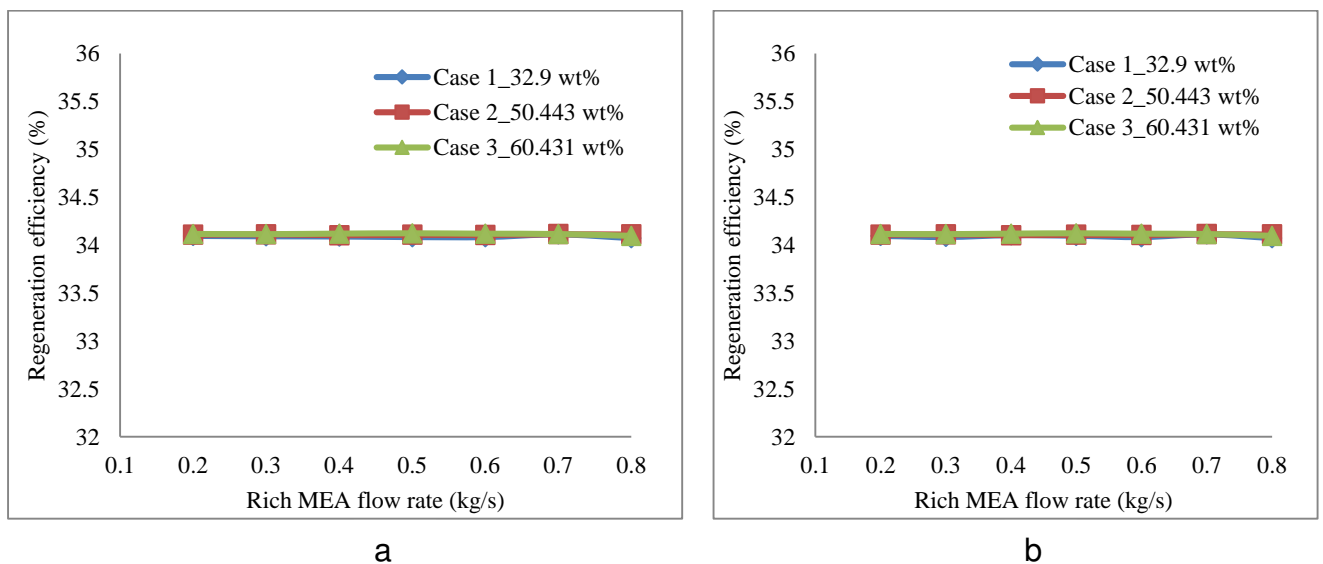
368 **Figure 3a** (using Equation 27) and **Figure 3b** (using Equation 28) show a constant
 369 regeneration efficiency as the rich-MEA flow rate increases, this is because the rich-
 370 MEA loading is the same for all the cases and the lean-MEA loading which is one of
 371 the output is controlled at the same value of 0.3178 mol/mol. **Figure 4a** presents the
 372 amount of CO₂ strip-off from the stripper as the rich-MEA flow rate increases. The
 373 graph shows an increase in the amount of CO₂ desorbed as the rich-MEA flow rate
 374 increases. This is attributed to increase in droplet flow regime. As liquid flowrate
 375 increases, the liquid breaks up more readily as they enter the rotating packing
 376 forming more droplets due to their higher velocity. Studies by Chambers and Walls
 377 [45] already showed that droplet flow regime in RPBs generally favours better mass
 378 transfer performance than the film flow regime. It is not surprising then that CO₂
 379 desorption rate noticeably increases (**Figure 4a**) as liquid flowrate increases. **Figure**
 380 **4a** also shows that higher MEA concentration gives higher CO₂ desorption rate. This
 381 is due to their higher loading capacity, which means the amount of CO₂ absorbed is
 382 more. Therefore, under similar conditions then, desorption rate from more
 383 concentrated MEA solution is expected to be more.

384 **Figure 4b** shows firstly that the residence time decreases with increasing liquid
 385 flowrate. To understand this, referring to Equations 31 and 32, it is seen that the
 386 residence time can be related to flowrate as follows (assuming other parameters in
 387 Equations 31 and 32 remain constant):

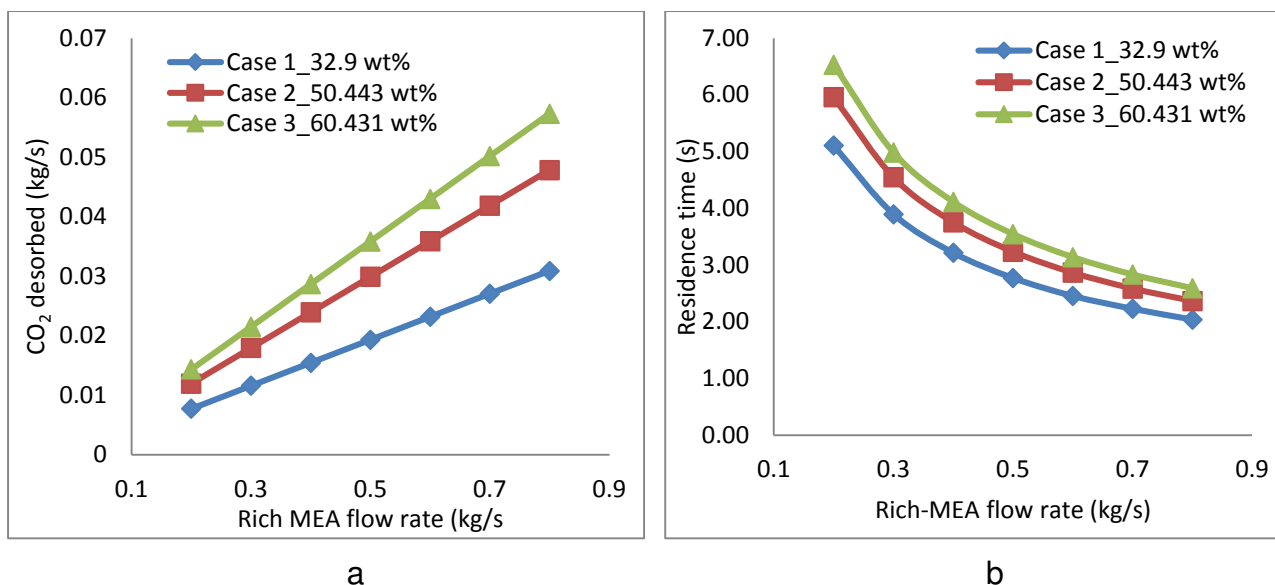
$$388 \quad t_{\text{res}} = KQ_L^{-\frac{2}{3}} \quad (33)$$

389 With K (= constant), this simply shows that increasing flowrate will result to lower
 390 residence time. In physical terms, this can be further explained by acknowledging
 391 that liquid velocity increases with flowrate. Higher liquid velocity means that delay
 392 within the system is less and this ultimately means lower residence time.

393 The other result shown in **Figure 4b** is increase in residence time as MEA solution
 394 concentration increases. This is due to increase in solution density (i.e. 1062.784
 395 kg/m³ for 32.6 wt%, 1162.062 kg/m³ for 50.443 wt%, 1209.465 kg/m³ for 60.431
 396 wt%) and viscosity (i.e. 0.000681235 N.s/m² for 32.6 wt%, 0.000990415 N.s/m² for
 397 50.443 wt%, 0.00125367 N.s/m² for 60.431 wt%).



398 Figure 3 Effect of rich-MEA flow rate on regeneration efficiency (a) using Equation 27
 399 (b) using Equation 28



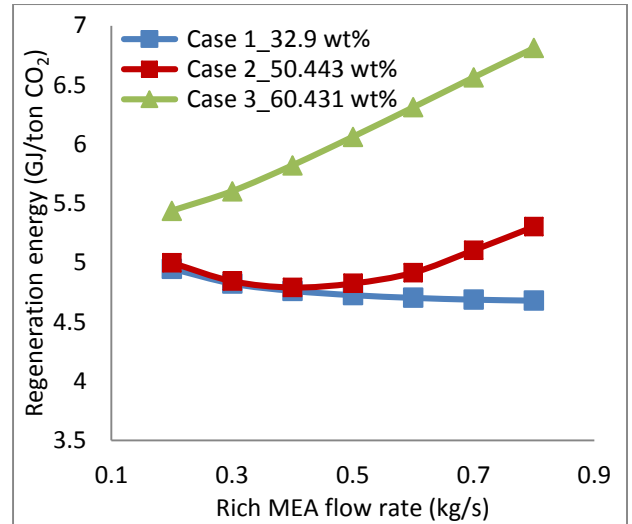
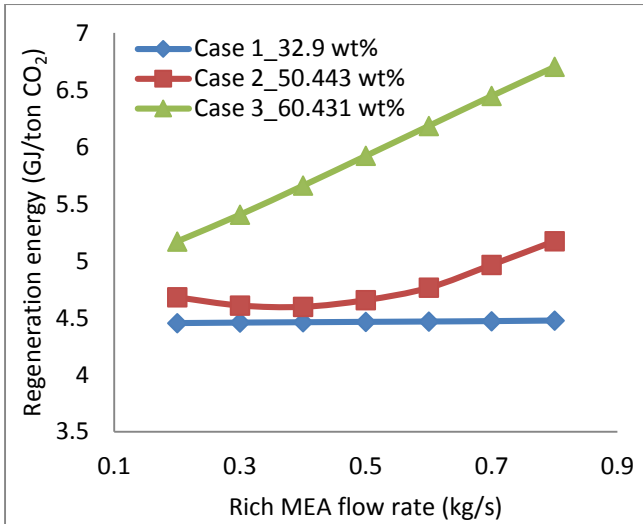
400

401 Figure 4 Effect of rich-MEA flow rate on (a) CO₂ desorbed (b) Residence time

402 It can be observed from **Figure 5a,b** that the regeneration energy increases with
 403 increase in rich-MEA flow rate for Cases 2 and 3 (with and without motor power). For
 404 Case 1 (without motor energy) the regeneration energy is fairly constant as the rich-
 405 MEA flowrate increases as shown in **Figure 5a**. This is because the percentage
 406 increase in the reboiler duty shown in **Figure 6** is same as the percentage in CO₂
 407 desorbed (**Figure 4a**) (i.e. 75.103% increase in reboiler duty and 74.973% increase
 408 in amount of CO₂ desorbed for Case 1) while for Case 2 there is 77.383% increase
 409 in reboiler duty and 75.003% increase in amount of CO₂ desorbed and Case 3 has
 410 80.703% increase in reboiler duty, 74.986% increase in amount of CO₂ desorbed.
 411 The lowest regeneration energy obtained from the study is at flow rate of 0.2 kg/s
 412 rich-MEA. For Case 3 the regeneration energy is 5.17 GJ/ton CO₂ (without motor
 413 energy) and 5.44 GJ/ton CO₂ (with motor energy). The highest regeneration energy
 414 for Case 2 is at rich-MEA flow rate of 0.8 kg/s and the regeneration energy is 5.17
 415 GJ/ton CO₂ (without motor energy) and 5.31 GJ/ton CO₂ (with motor energy). For
 416 Case 1 (with motor power) regeneration energy decreases with increase in rich-MEA
 417 flow.

418 The percentage increase in regeneration energy (i.e. including motor energy) when
 419 rich-MEA flowrate increases from 0.2 kg/s to 0.8 kg/s is 5.74% and 20.18% for
 420 Cases 2 and 3 respectively, while for Case 1 the regeneration energy decreases by
 421 5.72%.

422 Looking at **Figures 5a,b and 6**, one may wonder why higher MEA concentration
 423 solvent is preferred for the RPB technology when the energy consumption is higher.
 424 It should be noted that here it is for stripper only. For a closed loop process including
 425 RPB Absorber and RPB stripper, the recycling solvent flowrate would be much lower
 426 for higher concentration solvent for the same capture efficiency in the absorber.
 427 Thus the energy consumption will be lower.



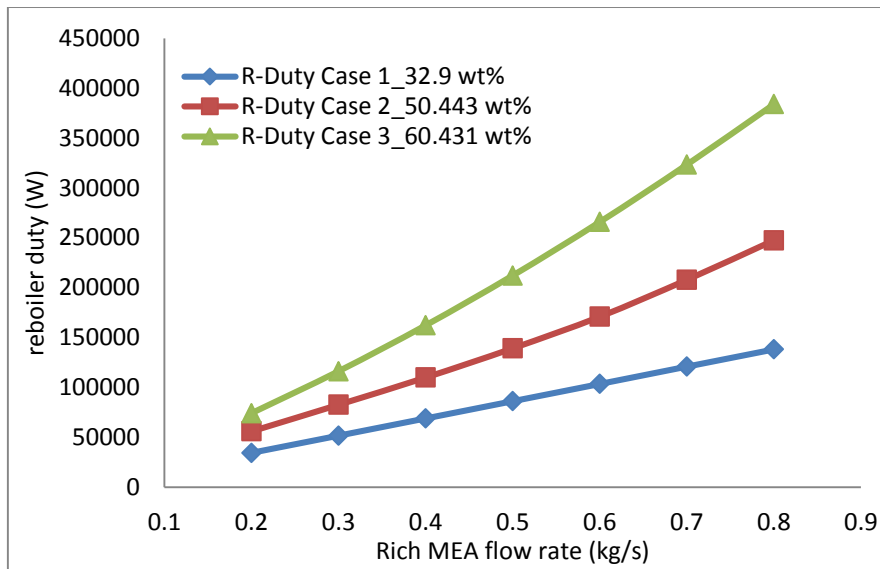
428

a

b

429 Figure 5 Effect of rich-MEA flow rate on regeneration energy (a) without motor
 430 energy (b) with motor energy

431

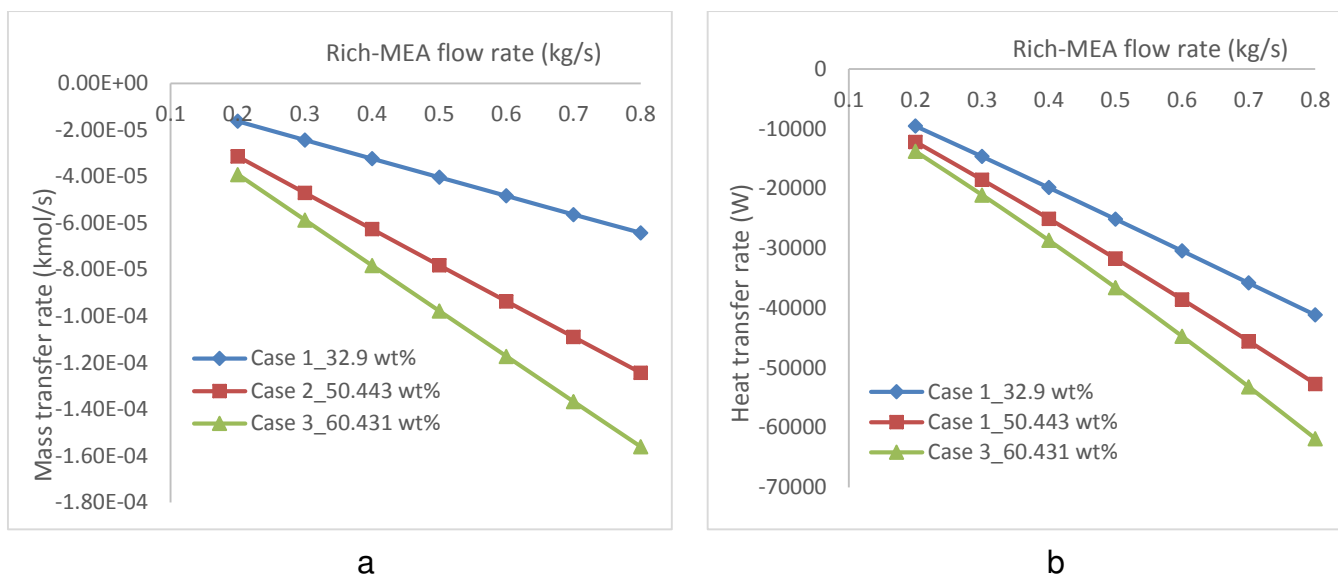


432

433

Figure 6 Effect of rich-MEA flow rate on reboiler duty

434

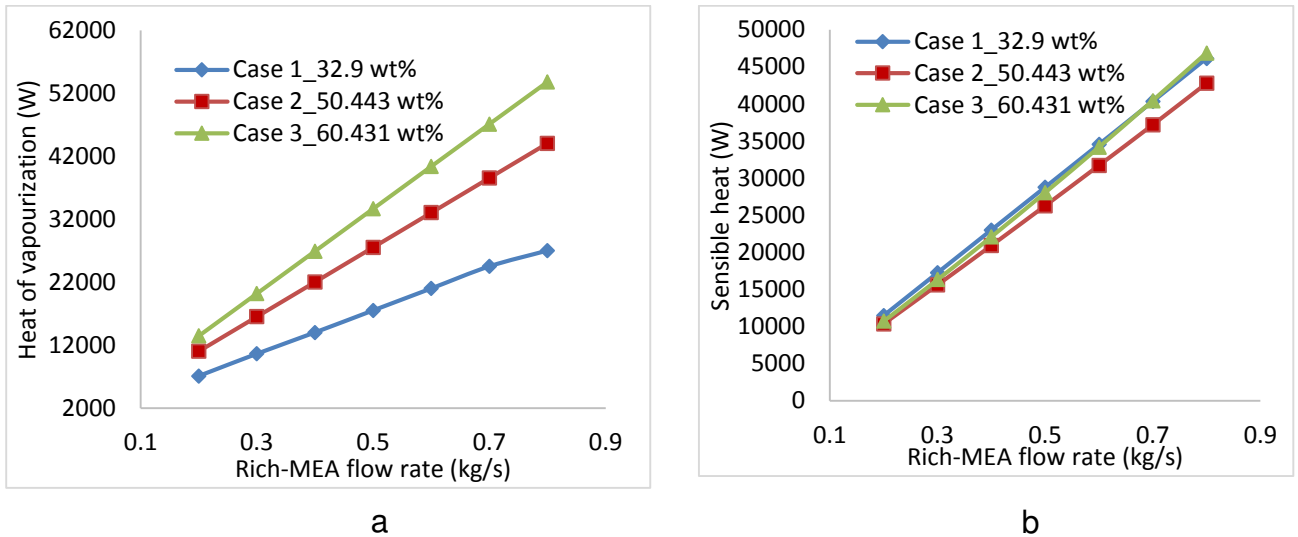


435 Figure 7 Effect of Rich-MEA flow rate on (a) mass transfer rate (b) heat transfer rate

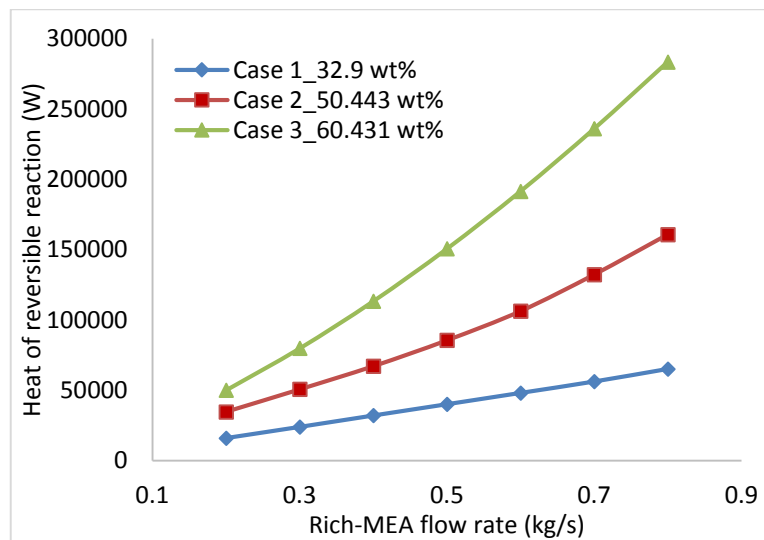
436 **Figure 7a** shows how the CO₂ mass transfer rate increases as the rich-MEA flow rate increases. Mass transfer is generally defined as transfer from either vapour to liquid or liquid to vapour. Here CO₂ is transferred from liquid to vapour, therefore
 437 negative sign appears. **Figure 7a** shows higher mass transfer rate for high MEA
 438 concentration this is because more CO₂ has been dissolve in it, therefore the rate of
 439 CO₂ desorbed will be higher than the lower MEA concentration. In **Figure 7b** heat
 440 transfer rate increases with increase in rich-MEA flow rate, the negative sign indicate
 441 transfer from liquid to vapour. The studies on CO₂ mass transfer rate and the heat
 442 transfer rate look at mass and heat transfer from the inner to outer radius of the RPB
 443 excluding the mass and heat transfer in the condenser and reboiler.
 444
 445

446 To further account for why there is an increase in the regeneration energy as shown
 447 in **Figures 5a,b**, the heat duty requirement in the reboiler is divided into three
 448 different parts: (i) Sensible heat to raise the temperature of the rich-MEA stream in
 449 the reboiler; (ii) Heat of reaction to reverse the absorption reaction and release CO₂;
 450 (iii) Heat of vapourisation to maintain the driving force for transfer of CO₂ from liquid
 451 phase to gas phase. **Figures 8a,b** and **9** show how the heat of vapourisation,
 452 sensible heat and the heat of reversible reaction increases with increase in rich-MEA
 453 flow rate respectively. **Figure 8a** shows that Heat of vapourisation is higher for high
 454 MEA concentration than lower MEA concentration this is due to the difference in their
 455 vapour composition (i.e. Case 1 has vapour composition of 0.25% H₂O, 97.13%
 456 MEA and Case 2 has 0.70% H₂O, 97.64% MEA and Case 3 has 1.49% H₂O,
 457 97.85% MEA). Sensible heat for the three Cases is almost the same this is because
 458 the rich-MEA flow rate coming into the stripper is same and the specific heat
 459 capacity is relatively same and the difference in the specific heat capacity is counter
 460 balanced by the temperature differences. **Figure 9** shows that heat of reversible
 461 reaction increases with increase in concentration this is as a result more energy
 462 needed to break the CO₂ and MEA bonds and because of the decrease in the
 463 amount of free CO₂ as the MEA concentration increases. **Figure 10** shows how the

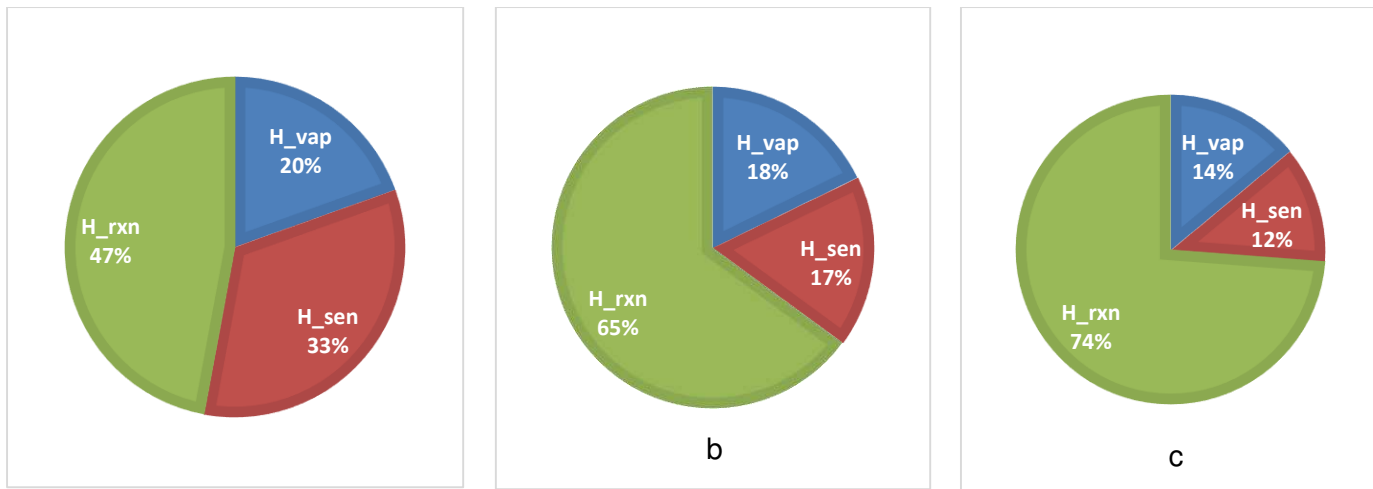
464 reboiler duty requirement was divided for a fixed rich-MEA flowrate of 0.8 kg/s at
 465 three different MEA concentrations. This shows that the heat of reaction increases
 466 from 47%, to 65% and 74% when rich-MEA concentration increases from 32.9 wt%,
 467 to 50.443 wt% and 60.431 wt%. This is consistent with amount of CO₂ stripped as
 468 presented in Figure 4 (a).
 469 Therefore, this study will help operators and designers of RPB regenerator to
 470 balance between energy consumption requirement and amount of CO₂ desorbed for
 471 a given Rich-MEA flow rate.



472 a b
 473 Figure 8 Effect of Rich-MEA flow rate on (a) Heat of vapourisation (b) Sensible heat



474
 475 Figure 9 Effect of Rich-MEA flow rate on heat of reversible reaction



476 Figure 10 Heat contributions for 0.8 kg/s rich-MEA flowrate at different MEA
 477 concentration (a) 32.9 wt% MEA (b) 50.443 wt% MEA (c) 60.431 wt% MEA

478 4.2 Effect of rotor speed on regeneration efficiency and regeneration energy

479 4.2.1 Justification for case study

480 The higher the rotating speed of the intensified regenerator the higher the energy
 481 consumed, therefore it is important to understand the relationship that rotor speed
 482 has with rich-MEA solvent flow rate so that the energy requirement for driving the
 483 stripper can be reduced with respect to the amount of rich-MEA solvent regenerated.

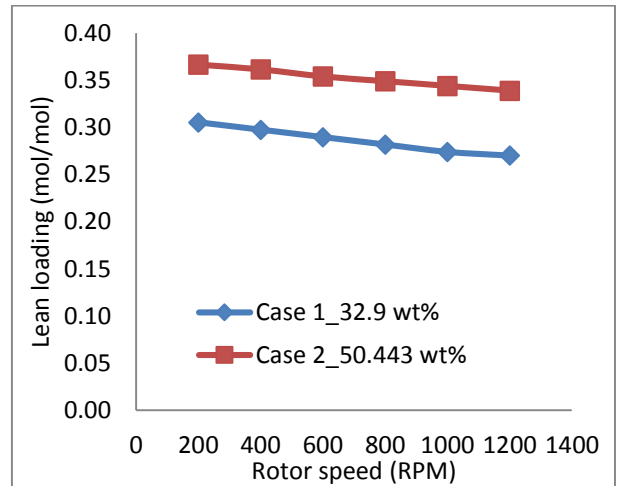
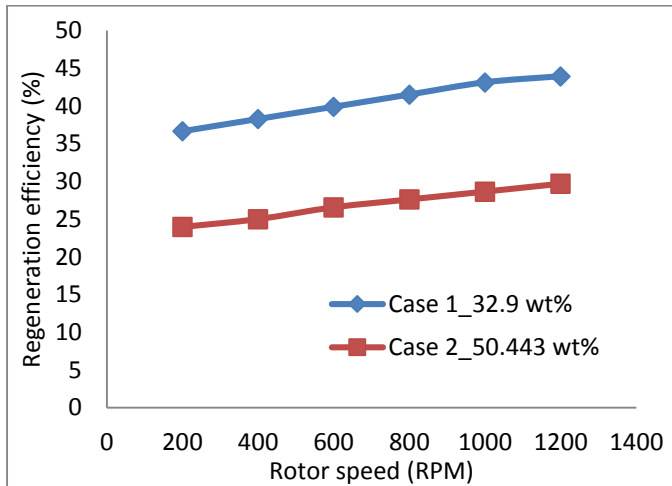
484 4.2.2 Setup of the case study

485 For this study, the rotor speed was varied from 200 rpm and 1200 rpm in order to
 486 cover the experimental range of rotor speed reported in Jassim *et al* [24] and Cheng
 487 *et al* [25]. Input process conditions for this study are shown in **Table 9** (i.e. Cases 1
 488 and 2). The reboiler temperature, rich-MEA flow rate and rich-MEA loading were kept
 489 constant at 120 °C 0.3 kg/s and 0.4823 mol/mol respectively for all the cases.

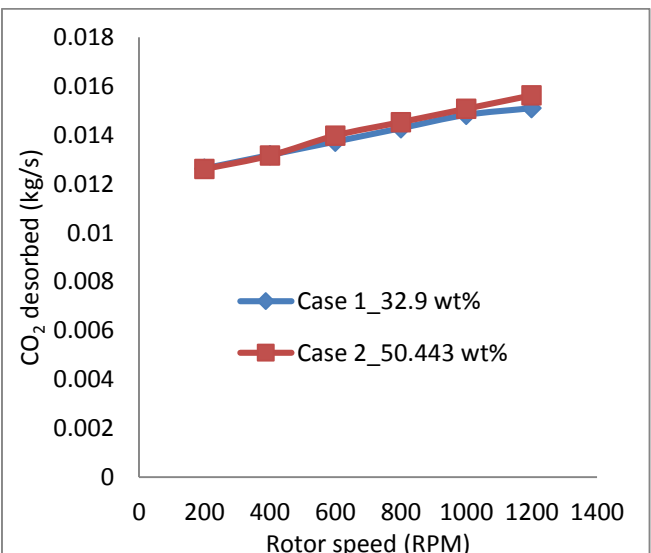
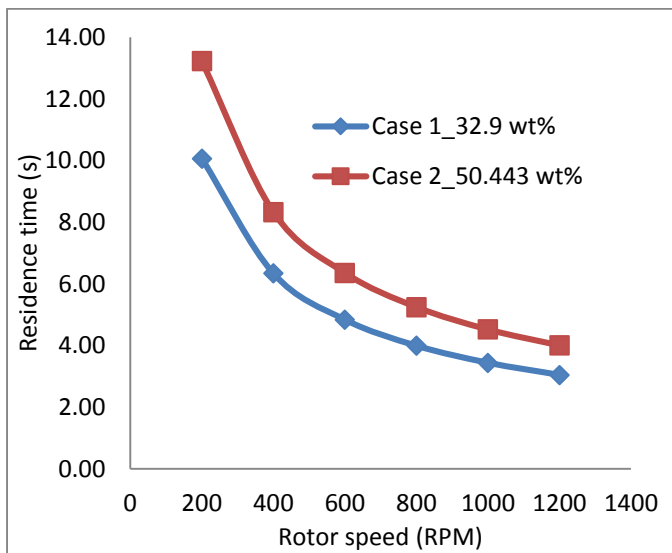
490 4.2.3 Results and discussion

491 **Figure 11a** shows that the regeneration efficiency increases with increase in the
 492 rotor speed. The impact of rotor speed on lean-MEA loading is shown in **Figure 11b**.
 493 Though higher rotor speed can produce opposite effect on mass and heat transfer by
 494 decreasing the residence time (as shown in **Figure 12a**) but this effect was counter
 495 balanced by the increase in the interfacial area which enhances mass and heat
 496 transfer. Burns *et al.* [46] stated that at higher rotor speed there are more of smaller
 497 liquid droplets and thinner liquid films in the packing regions of the bed, which means
 498 increase in interfacial area. The set-up in this study is different with the one reported
 499 in Section 4.1 where the lean-MEA loading was kept constant but in this study the
 500 recovery rate is kept constant for all the MEA concentrations, but the recovery rate

501 changes as the rotor speed increases. **Figure 11a** shows that regeneration
 502 efficiency decreases with increase in concentration this is because the rich-MEA
 503 loading is maintained at same value and the recovery rate is fixed at the same value
 504 for different rotor speed meaning that the change between rich-MEA loading to lean-
 505 MEA loading is smaller for higher MEA concentration than lower MEA concentration.
 506 The amount of CO₂ desorbed from the stripper increases as the rotor speed
 507 increases as shown in **Figure 12b**. The amount of CO₂ desorbed for the two
 508 different cases are similar this is due to the model set-up where the recovery rate
 509 were maintained at the same value but varied with rotor speed.



510 a b
 511 Figure 11 Effect of rotor speed on (a) regeneration efficiency (b) lean loading

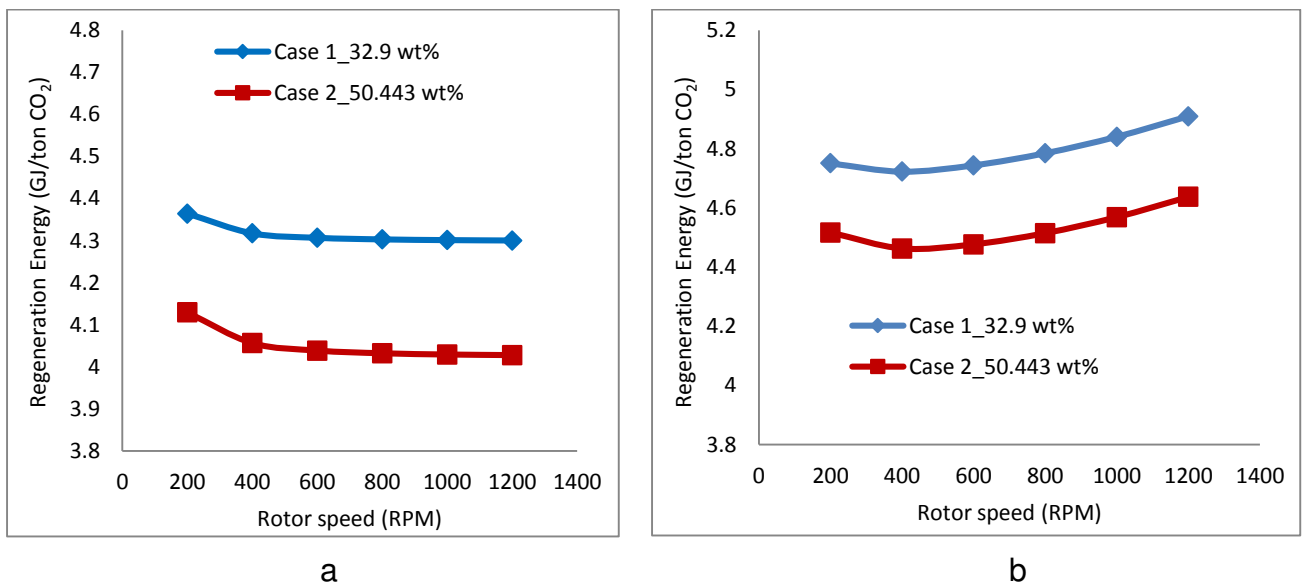


512 a b
 513 Figure 12 Effect of rotor speed on (a) residence time (b) CO₂ desorbed

514 Increase in rotor speed decreases the regeneration energy as shown in **Figure 13a**.
 515 This is because increase in rotor speed leads to more liquid droplet and thin liquid
 516 films to dominate the packing resulting in increase in mass and heat transfer. Also at

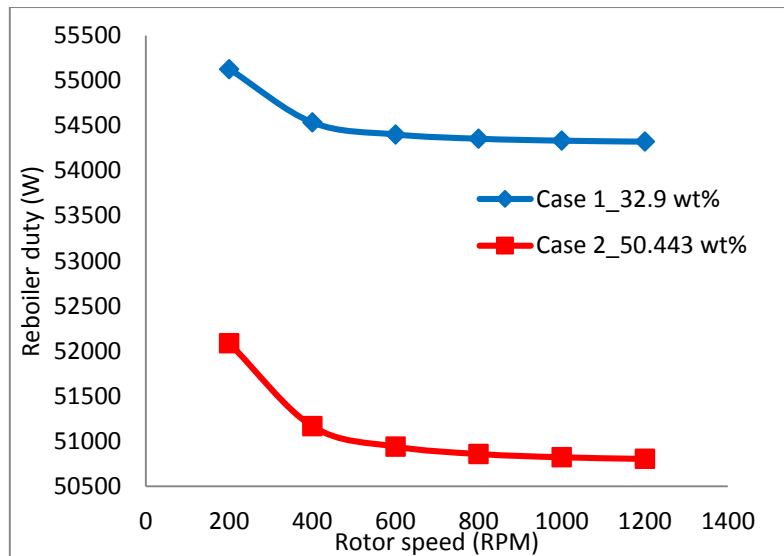
517 higher rotational speed the problem of liquid mal-distribution is overcome leading to
 518 higher wetted area which subsequently contributes to improving mass transfer. For
 519 all cases, the trend in **Figure 13a** (without motor energy) shows a drop in the
 520 regeneration energy as the rotor speed increases from 200 rpm to 1200 rpm this is
 521 because of increase in the rate of CO₂ stripped-off (**Figure 12b**). But when energy
 522 consumed by the motor is included **Figure 13b**, there is an increase in regeneration
 523 energy at rotor speed above 600 rpm for Case 2 and above 400 rpm for Case 1. This
 524 is because the motor energy is a function of square of rotor speed. Also **Figures**
 525 **13a,b** shows that regeneration energy decreases with increase in MEA
 526 concentration this is due to smaller difference between rich-MEA loading and lean-
 527 loading as seen in **Figure 11b** (i.e. at rotor speed of 600rpm Cases 1 and 2 has
 528 lean-MEA loading as an output from the model of 0.2898 mol/mol and 0.354076
 529 mol/mol respectively). The average percentage increase in regeneration energy
 530 when motor power is included is 6.44% and 6.84% for Case 1 and Case 2
 531 respectively. **Figure 14** shows how the reboiler duty increases with increase in rotor
 532 speed. Case 1 has higher reboiler duty because the difference in rich-MEA to lean-
 533 MEA loading is bigger which means higher reboiler duty, since reboiler duty is
 534 related to the difference in lean and rich loading.

535 This study will help operator and designer of RPB regenerator in chosen the rotor
 536 speed that give lower regeneration energy without compromising the amount of CO₂
 537 desorbed.



538

539 Figure 13 Effect of rotor speed on regeneration energy (a) without motor energy (b)
 540 with motor energy



541

542 Figure 14 Effect of rotor speed on reboiler duty

543

543 4.3 Effect of reboiler temperature on regeneration efficiency and energy

544

544 4.3.1 Justification for case study

545

545 Operating intensified regenerator at the right reboiler temperature will lead to good
 546 system performance by reducing regeneration energy waste and also operating at
 547 relatively high regeneration efficiency.

548

548 4.3.2 Setup of the case study

549

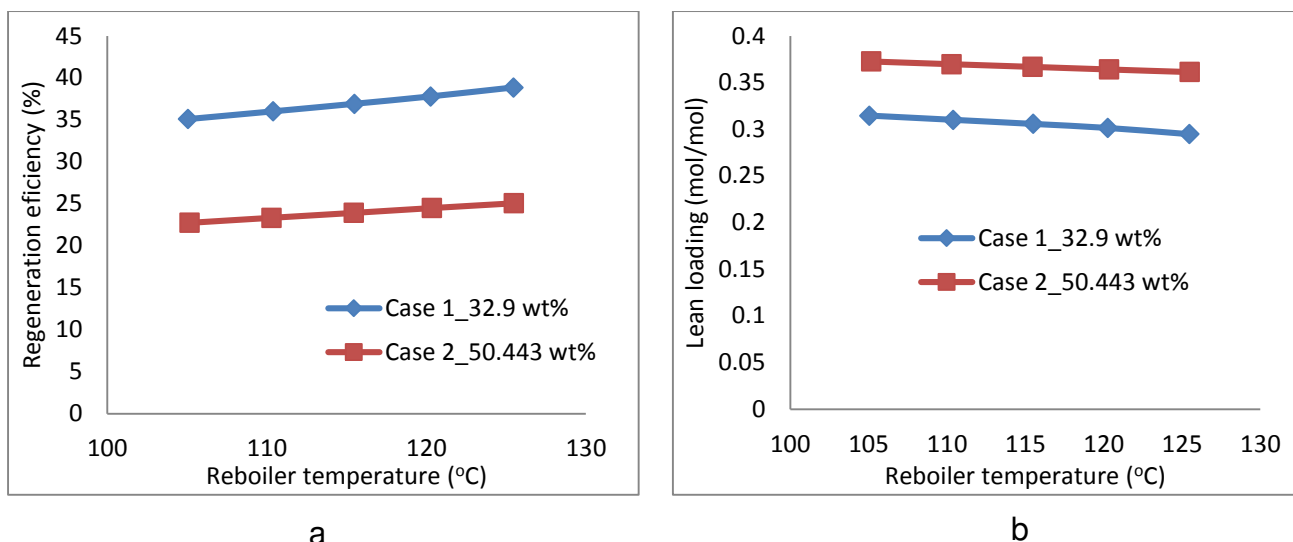
549 For this study, the reboiler temperature was varied from 105 to 125 °C. Process input
 550 conditions are same as in **Table 9** (i.e. Cases 1 and 2). The rich-MEA flow rate and
 551 rich-MEA loading were kept constant at 0.3 kg/s and 0.4823 mol/mol respectively for
 552 all the cases.

553

553 4.3.3 Results and discussion

554

554 **Figure 15a** shows that the regeneration efficiency increases with increase in reboiler
 555 temperature. The percentage increase in regeneration efficiency as the reboiler
 556 temperature increases for Cases 1 and 2 is about the same 9.67% and 9.33%
 557 respectively. The model shows that regeneration efficiency for Case 1 which has
 558 lower MEA concentration is higher. This is due to lower lean-MEA loading coming
 559 out as shown in **Figure 15b** since at each reboiler temperature for Case 1 and 2, the
 560 amount CO₂ desorbed is maintained at around the same value and also more CO₂
 561 was dissolved in higher MEA concentration than the lower MEA concentration in
 562 order to have the same rich-MEA loading coming into the stripper. **Figure 15b** shows
 563 that there is a decrease in lean-MEA loading as the reboiler temperature increases.
 564 This is because of increase in the amount of CO₂ stripped-off as shown in **Figure 16**.

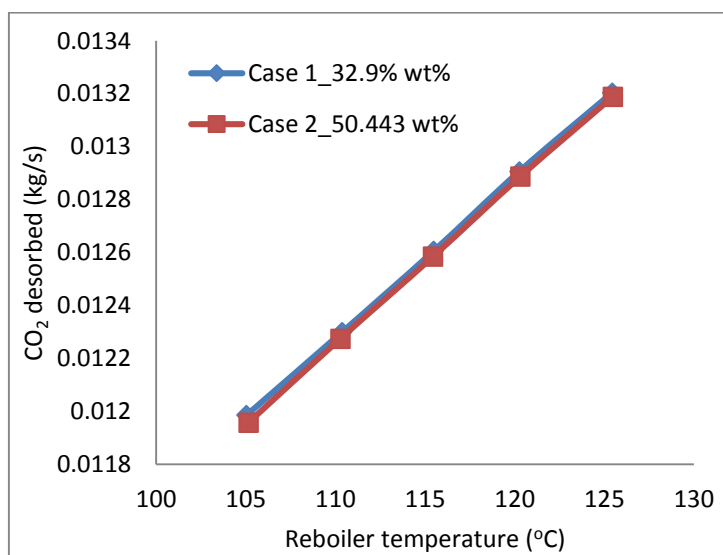


565

566

567

Figure 15 Effect of reboiler temperature on (a) regeneration efficiency (b) lean loading



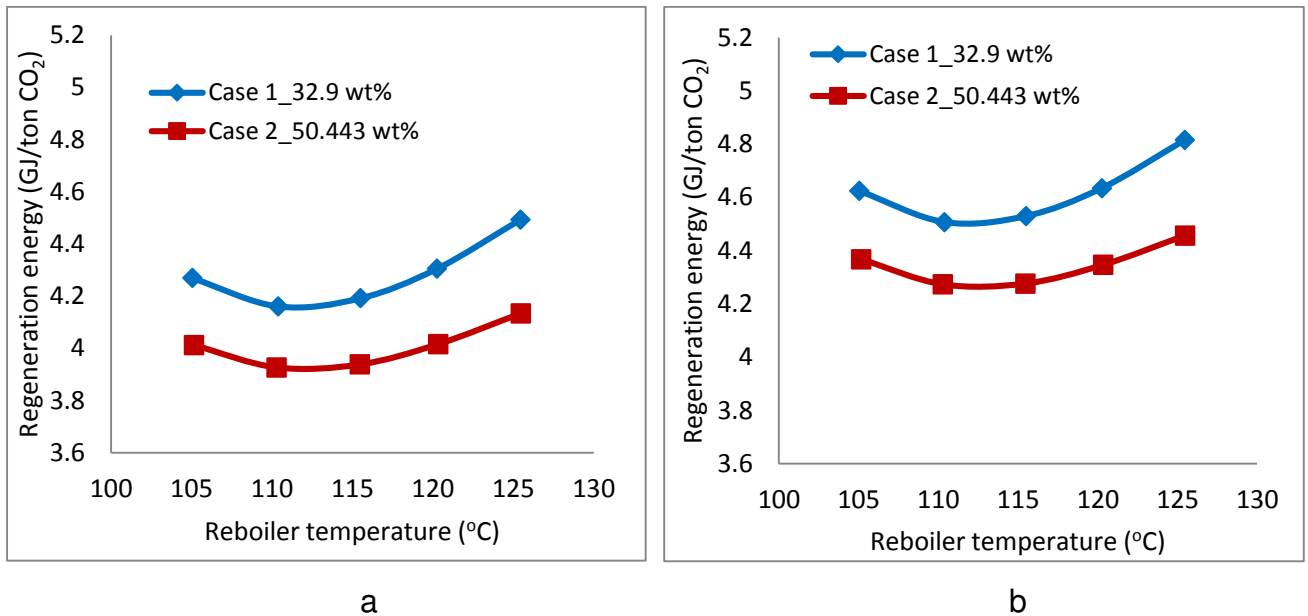
568

569

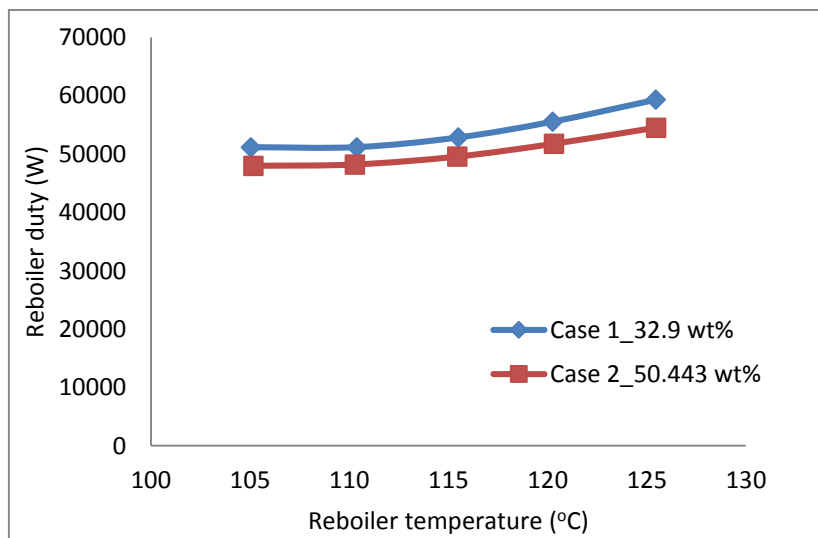
Figure 16 Effect of reboiler temperature on amount of CO₂ desorbed

570 There is a decrease and increase in regeneration energy as the reboiler temperature
 571 increases from 105 °C to 125 °C. From **Figure 16a,b** (with and without motor
 572 energy) the regeneration energy decreases as the reboiler temperature increases
 573 from 105 °C to 115 °C for Case 1 and 2, but this behaviour changes when the
 574 reboiler temperature exceed 115 °C. This is because at higher temperature we
 575 expect increase in water vapour flow rate which results in increase in regeneration
 576 energy because of heat of vaporisation of water. Also **Figure 19b** shows how the
 577 MEA composition in the vapour stream increases with increase in reboiler
 578 temperature this means increase in heat of vapourisation. Also from **Figure 15b** the
 579 loading different between the rich-MEA and lean-MEA stream is wide for Case 1
 580 than Case 2 that is why it has higher reboiler duty requirement. **Figure 18** shows
 581 how the reboiler duty increases with increase in reboiler temperature. The decrease

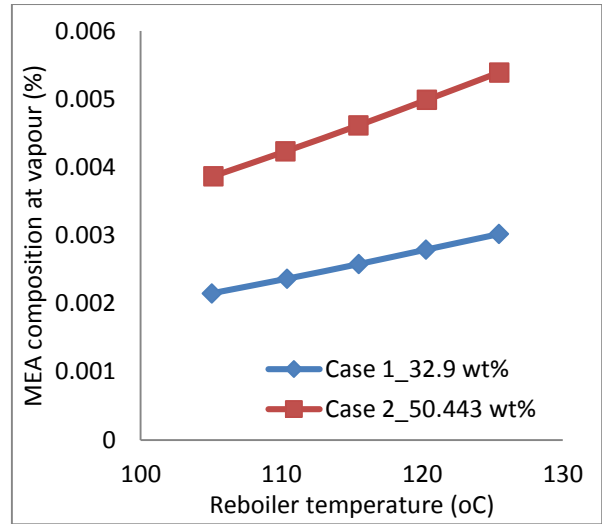
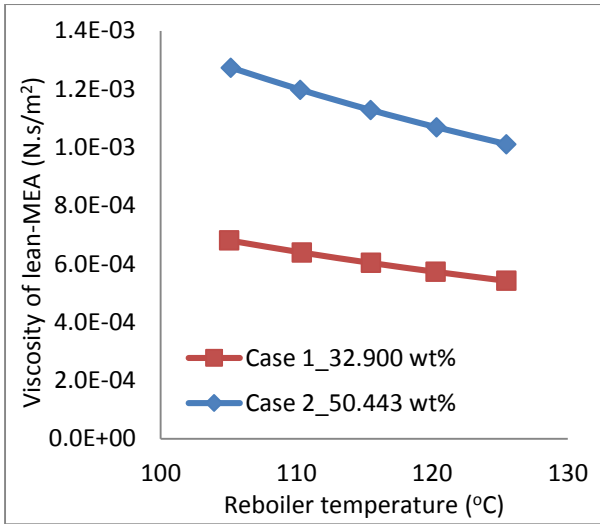
582 and increase in the regeneration energy can be further explained by **Figure 20 a,b**
 583 and **Figure 21** where the reboiler heat duty requirement is split into the heat of
 584 vapourisation, sensible heat and heat of reversible reaction. Increase in reboiler
 585 temperature leads to increase in heat of vapourisation and sensible heat while heat
 586 of reversible reaction decreases. The decrease in heat of reversible reaction is
 587 because of increase in rate of reaction as temperature increases.



588 a b
 589 Figure 17 Effect of reboiler temperature on regeneration energy (a) without motor
 590 energy (b) with motor energy
 591



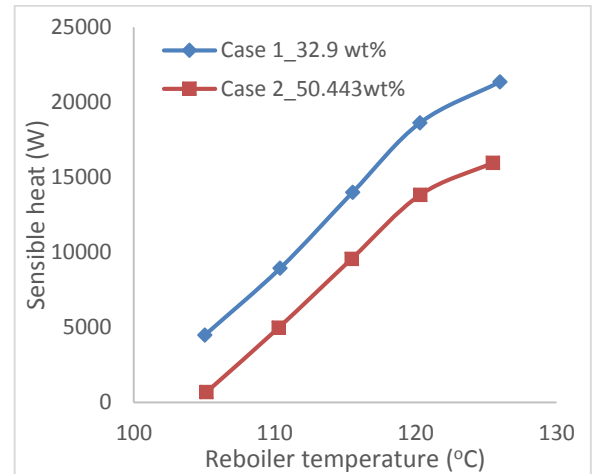
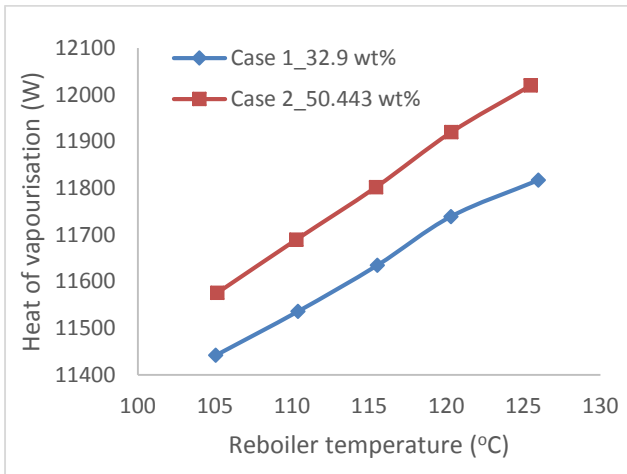
592
 593 Figure 18 Effect of reboiler temperature on reboiler duty



a

b

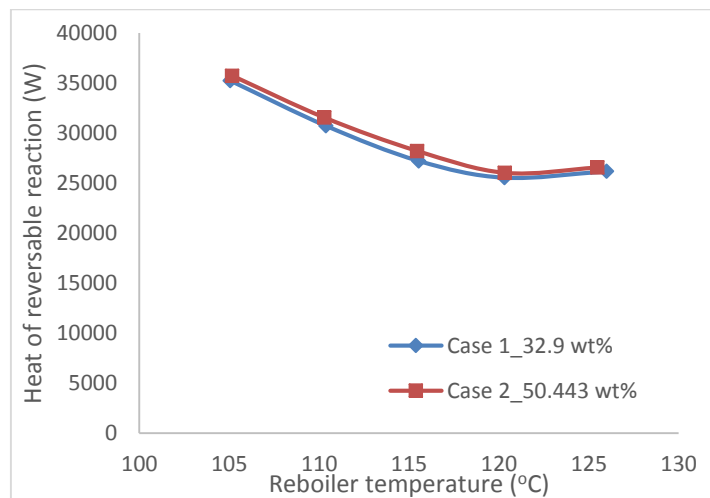
594 Figure 19 Effect of reboiler temperature on (a) lean-MEA viscosity (b) MEA content
595 in outlet vapour stream



a

b

596 Figure 20 Effect of reboiler temperature on (a) heat of vapourisation (b) sensible heat



597
598

Figure 21 Effect of reboiler temperature on heat of reversible reaction

599

600 **5 Comparison between RPB based intensified and PB based regenerator**

601 *5.1.1 Justification for the case study*

602 This study was carried out to provide a comparison under some fixed conditions
603 such as Rich-MEA flowrate, pressure, temperature, rich-MEA loading and lean-MEA
604 loading between intensified regenerator and conventional regenerator.

605 *5.1.2 Setup of the case study*

606 For this study, **Table 10** presents the input conditions for the conventional and
607 intensified regenerator. The rotor speed for the intensified regenerator is kept
608 constant at 1000 rpm. Regeneration efficiency was kept constant at 37.16 % for both
609 the conventional and the intensified regenerators.

610 Table 10 Process conditions for Conventional and RPB regenerator

Description	Conventional	RPB regenerator
	regenerator	
	R-MEA	Lean-MEA
Rich-MEA temperature (°C)	104	104
Rich-MEA pressure (kPa)	202.650	202.650
Rich-MEA flowrate (kg/s)	0.300	0.300
Rich-MEA loading (mol CO ₂ /mol MEA)	0.482	0.482
Mass-Fraction (wt%)		
H ₂ O	56.072	56.072
CO ₂	11.328	11.328
MEA	32.600	32.600

611 *5.1.3 Results and discussion*

612 The results in Table 11 show a 44 times packing volume reduction in RPB
613 regenerator compared to conventional PB regenerator without sumps. Using the
614 assumption given by Agarwal *et al.* [23] that the casing volume of RPB is 4.5 times
615 the rotating packing volume, the volume reduction compared to conventional PB
616 regenerator is found to be 9.691 times smaller. The height of transfer unit (HTU) for
617 conventional PB regenerator is calculated as 20.8 cm while for the RPB based
618 intensified regenerator is 1.7 cm. The smaller HTU in RPB regenerator leads to its
619 smaller size compared to conventional packed column. Wang *et al.* [20] performed
620 preliminary technical and economic analysis for intensified PCC process compared
621 with conventional PCC process. Initial prediction on the capital cost of the whole
622 intensified PCC process can reduce by 1/6 (i.e. 16.7%) compared with the same
623 capacity conventional PCC process. The 9.691 times reduction in the volume of

624 intensified regenerator reported here confirmed to the possibility of having 16.7%
 625 cost reduction for intensified PCC process.

626 Table 11 Comparison between conventional and RPB stripper

Description	Conventional PB regenerator	RPB regenerator
Height of packing (m)	3.700	0.371 (r _o) 0.152 (r _i)
diameter (m)	0.476	0.167 axial depth
Packing Volume (m ³)	0.659	0.015
Packing volume reduction		43.933 times
Volume of unit (m ³)	0.659 ^a	0.068 ^b
Volume reduction factor		9.691 times
Specific area (m ² /m ³)	151	2132
Void fraction	0.980	0.760
Lean-MEA loading (mol CO ₂ /mol MEA)	0.303	0.303

627 ^a Excluding sump

628 ^b Using the assumption given by Agarwal et al [23]

629

630 **6 Conclusions**

631 Intensified regenerator using RPB technology was modelled in this study. The steady
 632 state model was implemented by linking Aspen Plus[®] and visual FORTRAN. The
 633 model developed was validated with experimental data reported in Jassim *et al.* [24]
 634 and Cheng et al. [25]. The model validations show good agreement with the
 635 experimental data.

636 Process analysis on the effect of rich-MEA flow rate, rotational speed and
 637 reboiler temperature on CO₂ regeneration efficiency and regeneration energy
 638 were performed. For the given stripper (fixed in physical size), the study shows that
 639 an increase in the rich-MEA flow rate leads to an increase regeneration
 640 energy. There is an increase in the regeneration efficiency as the rotor speed
 641 increases but the regeneration energy decreases as the rotor speed increases
 642 since mass and heat transfer is enhanced at higher rotor speed. Reboiler
 643 temperature was varied from 105 °C to 125 °C, the results show a decrease in
 644 regeneration energy at reboiler temperature between 105 °C to 120 °C, but when the
 645 reboiler temperature exceeds 120 °C the regeneration energy begins to increase.
 646 Under the same process conditions, RPB based intensified stripper/regenerator has
 647 volume reduction of 9.691 times compared to conventional PB based
 648 stripper/regenerator. RPB stripper/regenerator shows great potential for application
 649 as a stripper and has much smaller size compared to conventional stripper which
 650 means reduction in capital cost.

651 **Acknowledgement**

652 The authors would like to acknowledge financial support from EPSRC Research
653 Challenges in Carbon Capture for CCS (Ref: EP/M001458/2) and EU FP7
654 International Staff Research Exchange Scheme on power plant and carbon capture
655 (Ref: PIRSES-GA-2013-612230).

656 **References**

657 [1] Department of Energy and Climate Change (DECC). Solid Fuels and Derived
658 Gases Statistics: Data Sources and Methodologies. 2012;Available at:
659 [http://webarchive.nationalarchives.gov.uk/20121217150421/http://decc.gov.uk/en/co](http://webarchive.nationalarchives.gov.uk/20121217150421/http://decc.gov.uk/en/content/cms/statistics/energy_stats/source/electricity/electricity.aspx)
660 [ntent/cms/statistics/energy_stats/source/electricity/electricity.aspx](http://webarchive.nationalarchives.gov.uk/20121217150421/http://decc.gov.uk/en/content/cms/statistics/energy_stats/source/electricity/electricity.aspx); (accessed
661 May,2013).

662 [2] Albo J, Luis P, Irabien A. Carbon dioxide capture from flue gases using a cross-
663 flow membrane contactor and the ionic liquid 1-ethyl-3-methylimidazolium
664 ethylsulfate. *Ind Eng Chem Res* 2010;49:11045-51.

665 [3] CO₂-Earth. Daily CO₂: Mauna Loa Observatory/ Atmospheric CO₂
666 Concentration
. Available at: [https://www co2 earth/daily-co2](https://www.co2earth.com/daily-co2) (accessed April,
667 2017).

668 [4] World Meteorological Organization (WMO). Press Release No. 991
. 26
669 May 2014;[http://www.wmo.int/pages/mediacentre/press releases/pr 991 en.html](http://www.wmo.int/pages/mediacentre/press_releases/pr_991_en.html)
670 (accessed June, 2014).

671 [5] Intergovernmental Panel on Climate Change (IPCC). Contribution of Working
672 Group III to the Fourth Assessment Report of the Intergovernmental Panel on
673 Climate Change. Cambridge, United Kingdom/New York, United States: Cambridge
674 University Press, 2007.

675 [6] International Energy Agency. Carbon Capture and Storage Model Regulatory
676 Framework. IEA 2010;Available at:
677 [http://www.iea.org/publications/freepublications/publication/model framework.pdf](http://www.iea.org/publications/freepublications/publication/model_framework.pdf),
678 (accessed May 2013).

679 [7] MacDowell N, Florin N, Buchard A, Hallett J, Galindo A, Jackson G et al. An
680 overview of CO₂ capture technologies. *Energy & Environmental Science*
681 2010;3:1645-69.

682 [8] Dugas RE. Pilot plant study of carbon dioxide capture by aqueous
683 monoethanolamine. MSE Thesis, University of Texas at Austin 2006.

684 [9] Lawal A, Wang M, Stephenson P, Obi O. Demonstrating full-scale post-
685 combustion CO₂ capture for coal-fired power plants through dynamic modelling and
686 simulation. *Fuel* 2012;101:115-28.

- 687 [10] Lawal A, Wang M, Stephenson P, Koumpouras G, Yeung H. Dynamic modelling
688 and analysis of post-combustion CO₂ chemical absorption process for coal-fired
689 power plants. *Fuel* 2010;89:2791-801.
- 690 [11] Lawal A, Wang M, Stephenson P, Yeung H. Dynamic Modeling and Simulation
691 of CO₂ Chemical Absorption Process for Coal-Fired Power Plants. *Computer Aided*
692 *Chemical Engineering* 2009;27:1725-30.
- 693 [12] Li K, Leigh W, Feron P, Yu H, Tade M. Systematic study of aqueous
694 monoethanolamine (MEA)-based CO₂ capture process: Techno-economic
695 assessment of the MEA process and its improvements. *Appl Energy* 2016;165:648-
696 59.
- 697 [13] Oh S, Binns M, Cho H, Kim J. Energy minimization of MEA-based CO₂ capture
698 process. *Appl Energy* 2016;169:353-62.
- 699 [14] Sharifzadeh M, Bumb P, Shah N. Carbon capture from pulverized coal power
700 plant (PCPP): Solvent performance comparison at an industrial scale. *Appl Energy*
701 2016;163:423-35.
- 702 [15] Hanak DP, Biliyok C, Manovic V. Efficiency improvements for the coal-fired
703 power plant retrofit with CO₂ capture plant using chilled ammonia process. *Appl*
704 *Energy* 2015;151:258-72.
- 705 [16] Zhao B, Liu F, Cui Z, Liu C, Yue H, Tang S et al. Enhancing the energetic
706 efficiency of MDEA/PZ-based CO₂ capture technology for a 650 MW power plant:
707 Process improvement. *Appl Energy* 2017;185, Part 1:362-75.
- 708 [17] Kvamsdal H, Jakobsen J, Hoff K. Dynamic modeling and simulation of a CO₂
709 absorber column for post-combustion CO₂ capture. *Chemical Engineering and*
710 *Processing: Process Intensification* 2009;48:135-44.
- 711 [18] Reay D. The role of process intensification in cutting greenhouse gas emissions.
712 *Appl Therm Eng* 2008;28:2011-9.
- 713 [19] Wang M, Lawal A, Stephenson P, Sidders J, Ramshaw C. Post-combustion CO₂
714 capture with chemical absorption: A state-of-the-art review. *Chem Eng Res Design*
715 2011;89:1609-24.
- 716 [20] Wang M, Joel AS, Ramshaw C, Eimer D, Musa NM. Process intensification for
717 post-combustion CO₂ capture with chemical absorption: A critical review. *Appl*
718 *Energy* 2015;158:275-91.
- 719 [21] Joel AS, Wang M, Ramshaw C, Oko E. Process analysis of intensified absorber
720 for post-combustion CO₂ capture through modelling and simulation. *International*
721 *Journal of Greenhouse Gas Control* 2014;21:91-100.
- 722 [22] Joel AS, Wang M, Ramshaw C. Modelling and simulation of intensified absorber
723 for post-combustion CO₂ capture using different mass transfer correlations. *Appl*
724 *Therm Eng* 2015;74:47-53.

- 725 [23] Agarwal L, Pavani V, Rao D, Kaistha N. Process intensification in HiGee
726 absorption and distillation: design procedure and applications. *Ind Eng Chem Res*
727 2010;49:10046-58.
- 728 [24] Jassim MS, Rochelle G, Eimer D, Ramshaw C. Carbon dioxide absorption and
729 desorption in aqueous monoethanolamine solutions in a rotating packed bed. *Ind*
730 *Eng Chem Res* 2007;46:2823-33.
- 731 [25] Cheng H, Lai C, Tan C. Thermal regeneration of alkanolamine solutions in a
732 rotating packed bed. *International Journal of Greenhouse Gas Control* 2013;16:206-
733 16.
- 734 [26] Zhao B, Su Y, Tao W. Mass transfer performance of CO₂ capture in rotating
735 packed bed: Dimensionless modeling and intelligent prediction. *Appl Energy*
736 2014;136:132-42.
- 737 [27] Chamchan N, Chang J, Hsu H, Kang J, Wong DSH, Jang S et al. Comparison of
738 rotating packed bed and packed bed absorber in pilot plant and model simulation for
739 CO₂ capture. *Journal of the Taiwan Institute of Chemical Engineers* 2017;73:20-6.
- 740 [28] Lin C, Lin Y, Tan C. Evaluation of alkanolamine solutions for carbon dioxide
741 removal in cross-flow rotating packed beds. *J Hazard Mater* 2010;175:344-51.
- 742 [29] Wang G, Xu Z, Yu Y, Ji J. Performance of a rotating zigzag bed—A new HIGEE.
743 *Chemical Engineering and Processing: Process Intensification* 2008;47:2131-9.
- 744 [30] BERR. Advanced power plant using high efficiency boiler/turbine. Report
745 BPB010. BERR, Department for Business Enterprise and Regulatory Reform.
746 2006; Available at:
747 [http://webarchive.nationalarchives.gov.uk/20090609003228/http://www.berr.gov.uk/fil](http://webarchive.nationalarchives.gov.uk/20090609003228/http://www.berr.gov.uk/files/file30703.pdf)
748 [es/file30703.pdf](http://webarchive.nationalarchives.gov.uk/20090609003228/http://www.berr.gov.uk/files/file30703.pdf) (accessed August 2015).
- 749 [31] Kothandaraman A, Nord L, Bolland O, Herzog HJ, McRae GJ. Comparison of
750 solvents for post-combustion capture of CO₂ by chemical absorption. *Energy*
751 *Procedia* 2009;1:1373-80.
- 752 [32] Chen Y, Lin F, Lin C, Tai CY, Liu H. Packing characteristics for mass transfer in
753 a rotating packed bed. *Ind Eng Chem Res* 2006;45:6846-53.
- 754 [33] Chen Y. Correlations of mass transfer coefficients in a rotating packed bed. *Ind*
755 *Eng Chem Res* 2011;50:1778-85.
- 756 [34] Luo Y, Chu G, Zou H, Zhao Z, Dudukovic MP, Chen J. Gas–liquid effective
757 interfacial area in a rotating packed bed. *Ind Eng Chem Res* 2012;51:16320-5.
- 758 [35] Burns J, Jamil J, Ramshaw C. Process intensification: operating characteristics
759 of rotating packed beds—determination of liquid hold-up for a high-voidage
760 structured packing. *Chemical Engineering Science* 2000;55:2401-15.

- 761 [36] Llerena-Chavez H, Larachi F. Analysis of flow in rotating packed beds via CFD
762 simulations—Dry pressure drop and gas flow maldistribution. *Chemical Engineering*
763 *Science* 2009;64:2113-26.
- 764 [37] Kang J, Sun K, Wong DS, Jang S, Tan C. Modeling studies on absorption of
765 CO₂ by monoethanolamine in rotating packed bed. *International Journal of*
766 *Greenhouse Gas Control* 2014;25:141-50.
- 767 [38] AspenTech. Aspen Physical Properties System – Physical Property Methods.
768 2010, Available at: <http://support.aspentech.com/> (accessed May 2014).
- 769 [39] Zhang Y, Chen C. Modeling CO₂ Absorption and Desorption by Aqueous
770 Monoethanolamine Solution with Aspen Rate-based Model. *Energy Procedia*
771 2013;37:1584-96.
- 772 [40] Tung H, Mah RS. Modeling liquid mass transfer in hige separation process.
773 *Chem Eng Commun* 1985;39:147-53.
- 774 [41] Onda K, Sada E, Takeuchi H. Gas absorption with chemical reaction in packed
775 columns. *J Chem Eng Japan* 1968;1:62-6.
- 776 [42] Sandilya P, Rao D, Sharma A, Biswas G. Gas-phase mass transfer in a
777 centrifugal contactor. *Ind Eng Chem Res* 2001;40:384-92.
- 778 [43] Singh SP, Wilson JH, Counce RM, Lucero AJ, Reed GD, Ashworth RA et al.
779 Removal of volatile organic compounds from groundwater using a rotary air stripper.
780 *Ind Eng Chem Res* 1992;31:574-80.
- 781 [44] Jassim MS. Process intensification: absorption and desorption of carbon dioxide
782 from monoethanolamine solutions using Hige technology. Newcastle University, UK
783 (PhD Thesis) 2002.
- 784 [45] Chambers H, Wall M. Some factors affecting the design of centrifugal gas
785 absorbers. *Trans.Inst.Chem.Eng* 1954;32:S96-S107.
- 786 [46] Burns J, Ramshaw C. Process intensification: visual study of liquid
787 maldistribution in rotating packed beds. *Chemical Engineering Science*
788 1996;51:1347-52.
- 789